Electronic Supplementary Material (ESI) for Organic Chemistry Frontiers.

Supplementary Information

Rescuing solid-state fluorescence of perylene diimide dyes by host-guest isolation

Yanfeng He,† Caihong Mao,† Mingwan Duan, Linmeng Fan, Xiaohan Wang, Yan Cai, Min Du, Minli Hu, Ping Hu, Qiuyu Cheng, and Xiaobo Hu*

Key Laboratory of the Ministry of Education for Advanced Catalysis Materials, College of Chemistry and Life Sciences, Zhejiang Normal University, 688 Yingbin Road, Jinhua 321004, P. R. China

[†] These authors contributed equally to this work.

* E-mail: xiaobo.hu@zjnu.edu.cn

Table of contents

Materials, methods, and abbreviations

Materials

All commercially available starting materials and reagents were used without further purification. Anhydrous solvents were obtained from commercial sources. **PDI-C8**, **PDI-C13**, **PDI-Ph** and **PDI-red** were purchased from Macklin Inc. China or Shanghai Aladdin Biochemical Technology. Analytical thin layer chromatography (TLC) was performed on silica gel plates (Merck 60F254) visualized with a UV lamp (254 nm). Column chromatography was performed with commercial glass columns using silica gel 200 - 300 mesh (particle size 0.045 - 0.075 mm).

Preparation of drop-cast films

Square glass with the size of 18 mm × 18 mm × 0.15 mm was used as the substrate. The stock solutions of PDI dyes, **1** and **TTP** were prepared with chloroform as the solvent at the concentrations of 1 mM, 1 mM and 5.5 mM, respectively. Note: for **PDI-Ph**, it was a suspension, but it could turn to a solution once diluted and mixed with **1**; the concentration of **TTP** is 5.5 times as big as that of **1** so that the mass concentration of **TTP** is equal to that of **1**. For the production of the drop-cast films, 80 uL of the stock solution was used for each sample to make sure each group contained the same amount of PDI dyes. For the samples with two components, two stock solutions were mixed together first and then 160 uL of the newly generated solution was used. Each film was dried first under atmosphere and then under vacuum to get rid of the solvents. Each sample was analyzed within two days and was stored in dark when not in use. The thickness of samples are ~ 1 μm (determined by a step gauge, Alpha-Step03010501). Please notice that this value provided here is just to give a rough idea of the thickness.

Preparation of powder samples

PDI dyes, TTP and **1** were dissolved in $CHCl_3$ as the stock solutions. PDI+**1** and PDI+**TTP** solutions were prepared by mixing the corresponding stock solutions together with the molar ratio of PDI to **1** as 1 : 1 and PDI to **TTP** as 1 : 5.5. Then, the solvent of the solutions of PDI,

PDI+**1** and PDI+**TTP** was evaporated at room temperature to afford the resulting powder samples.

UV-vis spectroscopy

UV-vis absorption spectra of solutions were recorded on a T6 new century spectrometer with a data interval of 1 nm. Conventional quartz cells with 1 mm and 10 mm path length were used throughout the study. UV-vis absorption spectra of films were recorded on a T9 new century spectrometer and the absorbance of film sample is in the linear range of the instrument (0.1 ~ 1.0).

Powder X-ray diffraction

X-ray diffraction measurement was performed on D8 Advance Bruker AXS X-ray diffractometer and the scanning range is 5° to 50° at a step size of 0.020°, 2197 steps, and 0.10 s per step.

Fourier transform infrared spectra

Fourier transform infrared spectra were recorded on iS5 Thermo Fisher at a resolution of 4 cm^{-1} with 16 scans over the range of 4000-500 cm^{-1}.

Fluorescence spectroscopy

Fluorescence spectra were recorded on an Edinburgh Instruments FLS 980 spectrometer with Xenon Xe1+400 nm lamp and visible PMT detector under following conditions: Dwell time = 0.05 s, step = 1 nm, number of scans = 1, without polarizers. Absolute quantum yields were measured using the integrating sphere assembly of FLS 980. Fluorescence lifetimes were recorded on the FLS 980 using an Edinburgh Instruments picosecond pulsed diode laser (EPL-450 nm, 200 ns or 500 ns, 5 or 2 MHz repetition rate). The detailed conditions for each sample are as follows: excitation wavelength (Ex.) 510 nm, excitation bandwidth (ExBW.) 1.6, 0.9, 2.2 nm and emission bandwidths (EmBW.) 1.3, 0.6, 2.1 nm with a 530 nm filter for emission spectra

of **PDI-C8, PDI-C8 + 1**, and **PDI-C8 + TTP**, respectively; Ex. 510 nm, ExBW. 1.9, 1.2, 2.0 nm and EmBW. 1.8, 1.0, 1.8 nm with a 530 nm filter for emission spectra of **PDI-C13, PDI-C13 + 1**, and **PDI-C13 + TTP**, respectively; Ex. 510 nm, ExBW. 2.5, 1.5, 2.0 nm and EmBW. 2.2, 1.2, 2.0 nm with a 530 nm filter for emission spectra of **PDI-Ph, PDI-Ph + 1**, and **PDI-Ph + TTP**, respectively; Ex. 510 nm, ExBW. 1.2, 0.8, 0.8 nm and EmBW. 1.2, 0.5, 0.8 nm with a 530 nm filter for emission spectra of **PDI-branch, PDI-branch + 1**, and **PDI-branch + TTP**, respectively; Ex. 510 nm, ExBW. 1.0, 0.5, 1.0 nm and EmBW. 0.8, 0.5, 0.5 nm with a 530 nm filter for emission spectra of **PDI-red, PDI-red + 1**, and **PDI-red + TTP**, respectively; Em. 633 nm, ExBW. 1.5, 1.0, 2.0 nm and EmBW. 1.3, 0.6, 2.0 nm with a 590 nm filter for excitation spectra of **PDI-C8, PDI-C8 + 1**, and **PDI-C8 + TTP**, respectively; Em. 640 nm, ExBW. 2.0, 1.0, 1.2 nm and EmBW. 1.5, 1.0, 1.2 nm with a 590 nm filter for excitation spectra of **PDI-C13, PDI-C13 + 1**, and **PDI-C13 + TTP**, respectively; Em. 630 nm, ExBW. 2.5, 1.5, 2.0 nm and EmBW. 2.0, 1.0, 1.8 nm with a 590 nm filter for excitation spectra of **PDI-Ph, PDI-Ph + 1**, and **PDI-Ph + TTP**, respectively; Em. 613 nm, ExBW. 1.2, 0.6, 0.8 nm and EmBW. 1.0, 0.5, 0.7 nm with a 590 nm filter for excitation spectra of **PDI-branch, PDI-branch + 1**, and **PDI-branch + TTP**, respectively; Em. 620 nm, ExBW. 0.6, 0.8, 0.8 nm and EmBW. 0.5, 0.7, 0.6 nm with a 590 nm filter for excitation spectra of **PDI-red, PDI-red + 1**, and **PDI-red + TTP**, respectively.

Mass spectrometry

High resolution electrospray ionization time-of-flight (HRESI-TOF) mass spectra were measured in the positive ion mode on a Agilent 6230 mass spectrometer.

NMR spectroscopy

^{1}H NMR spectra were recorded on a Bruker Avance III HD 400 in $CDCl_3$, DMSO-d_6 or 2% DMSO-d_6/$CDCl_3$. Chemical shifts are reported in ppm relative to residual solvent signal of $CDCl_3$ (δ = 7.26 ppm), DMSO-d_6 (δ = 2.50 ppm), or to TMS in 2% DMSO-d_6/$CDCl_3$ (δ = 0.00 ppm). Abbreviations used for signal multiplicity are: s = singlet, d = doublet, t = triplet, q = quartet, m = multiplet or overlap of nonequivalent resonances, br = broad. Coupling constants, J, are reported in Hertz (Hz). ^{13}C{^{1}H} NMR spectra were recorded on a Bruker AVANCE III HD

400 in $CDCl_3$ or DMSO-d_6 and the observed signals are reported in ppm relative to the residual solvent signal of $CDCl_3$ (δ = 77.16 ppm) or DMSO-d_6 (δ = 39.52 ppm). 2D NMR spectra were recorded on a Bruker AVANCE III HD 600 in 2% DMSO-d_6/$CDCl_3$.

2D NMR parameters.

Spectra of nuclear overhauser effect spectroscopy (NOESY) and correlation spectroscopy (COSY) experiments were recorded on a Bruker Avance III HD 600 by means of a 5 mm BBFO probe with z gradient. Data processing was performed with Topspin software. ^{1}H-^{1}H NOESY acquisition was performed with a time domain size of 2048 (F2) × 1024 (F1), 64 scans per increment, a pulse program of noesygpph, and a mixing time of 300 ms. ^{1}H-^{1}H COSY acquisition of **1** was performed with a time domain size of 2048 (F2) × 512 (F1), 8 scans per increment, and a pulse program of cosygpppgf.

Molecular modeling

MacroModel (Schrödinger Inc.) was used for building the molecular models based on the ^{1}H-^{1}H NOESY spectrum. The minimization conditions are as follows throughout the modeling: force field MMFFs; solvent, none; cutoff, extended; method, TNCG; and maximum iterations, 500. To begin, an opened and separated structure of PDI + **1** was employed to perform energy minimization by importing four distance constraints converted from the NOE correlations between amide protons (H_2) of **1** and perylene protons of PDI (H_b) to yield a intermediate structure (table S1 and figure S19). Then, the intermediate structure was further energy minimized by importing full (28) distance constraints from the key NOE correlations between **1** and PDI to give the final **PDI-C8⊂1** complex structure. With the first NMR structure in hand, another 19 NMR models were obtained to estimate the stability of the core structure and the freedom of the side functional groups. To access the other 19 molecular models, the same process as the first one was applied but each time with a different starting structure.

Abbreviations

HBTU = (2-(*1H*-benzotriazol-1-yl)-1,1,3,3-tetramethyluronium hexafluorophosphate; DIPEA = *N,N*-diisopropylethylamine; DCM = dichloromethane; DMSO = dimethyl sulfoxide; THF = tetrahydrofuran; PE = petroleum ether; EA = ethyl acetate.

Synthesis and characterization

Compounds **2**[1], **4**[2] and **PDI-branch**[3] are literature known and synthesized according to the reported procedures.

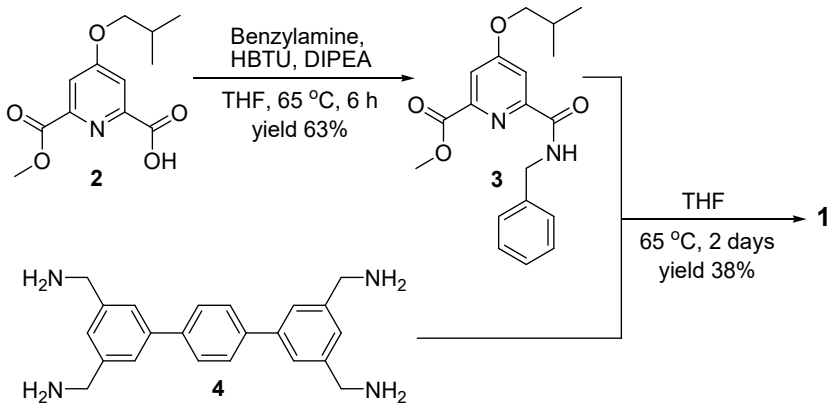

Scheme S1. Synthesis of the host **1**.

Synthesis of methyl 6-(benzylcarbamoyl)-4-isobutoxypicolinate (**3**)

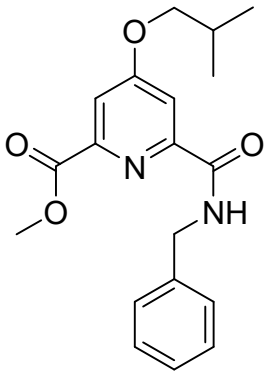

(methoxycarbonyl)-4-(3-methylbutan-2-yloxy) picolinic acid (4.2 g, 16 mmol), Benzylamine (2.2 ml, 20 mmol and HBTU (12.6 g, 33 mmol) were dissolved in 100 mL anhydrous THF, followed by addition of DIPEA (5.7 mL, 33 mmol) under N_2 at 65°C. The mixture was allowed to stir at 65°C for 6 h. Solvent was evaporated under vacuum and the crude product was washed with 1 mM hydrochloric acid to remove DIPEA. Column chromatography (eluent: PE/EA= 6/1, 4/1, 3/1) was performed to yield the title compound as a white amorphous solid (3.6 g, 63%). ^{1}H NMR (400 MHz, $CDCl_3$): δ (ppm) = 8.48 (t, J = 6.4 Hz, 1H), 7.90 (d, J = 2.4 Hz, 1H), 7.70 (d, J = 2.4 Hz, 1H), 7.40–7.26 (m, 5H), 4.69 (d, J = 6.0 Hz, 2H), 3.96 (s, 3H), 3.91 (d, J = 6.8 Hz, 2H), 2.19-2.10 (m, 1H), 1.05 (d, J = 6.4 Hz, 6H),. ^{13}C{^{1}H} NMR (400 MHz, CDCl3): δ (ppm) = 167.6, 165.1, 163.7, 152.0, 148.1, 138.2, 128.9, 127.9, 127.5, 114.8, 111.0, 75.2, 52.9, 43.5, 28.0, 19.1. HRMS (ESI): m/z calcd for $C_{19}H_{22}N_2O_4$ $[M+H]^+$: 343.1652, found: 343.1643. Melting point: 95.5 - 97.4 °C.

Elemental Analysis: predicted: C, 66.65%; H, 6.48%; N, 8.18%; found: C, 66.93%; H, 6.13%; N, 8.26%.

Synthesis of the host **1**

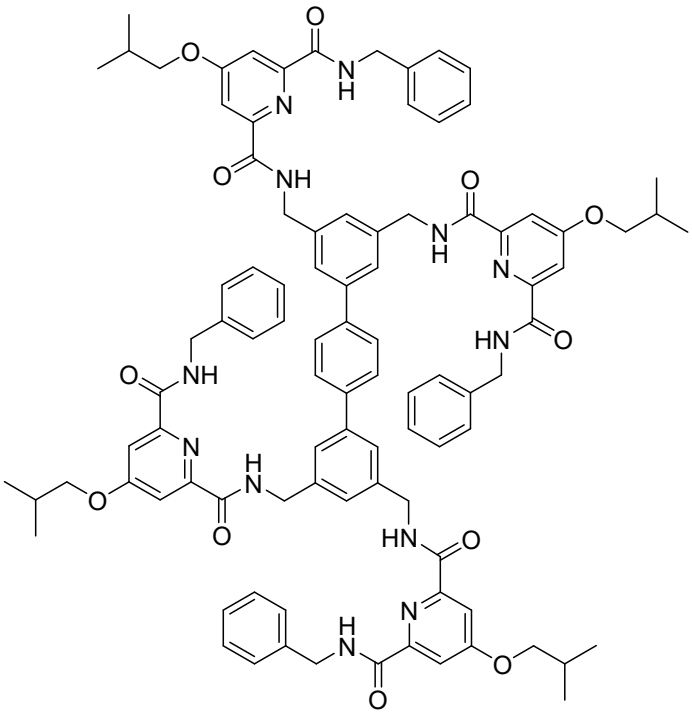

Compound **4** (200 mg, 0.57 mmol) was dissolved in 2 mL anhydrous THF followed by addition of **3** (889 mg, 2.59 mmol). The mixture was stirred at 65 °C for 2 days. Then solvent was evaporated under vacuum. The crude product was further purified by column chromatography (eluent: DCM/MeOH = 96/4, v/v%) to yield the title compound as a white amorphous solid (350 mg, 38%). ^{1}H NMR (400 MHz, DMSO-d_6): δ (ppm) = 9.87 (t, J = 6.4 Hz, 4H), 9.78 (t, J = 6.4 Hz, 4H), 7.67 (s, 4H), 7.65 (d, J = 2.4 Hz, 4H), 7.61 (d, J = 2.4 Hz, 4H), 7.55 (s, 4H), 7.33-7.17 (m, 22H), 4.65 (d, J = 6.0 Hz, 8H), 4.54 (d, J = 6.0 Hz, 8H), 3.96 (d, J = 6.4 Hz, 8H), 2.14–1.96 (m, 4H), 1.01 (d, J = 6.8 Hz, 24H). ^{13}C{^{1}H} NMR (400 MHz, DMSO-d_6): δ (ppm) = 167.2, 163.2, 163.1, 156.5, 150.6, 140.3, 139.3, 139.1, 128.3, 127.1, 126.84, 126.76, 123.9, 110.2, 110.2, 74.3, 42.1, 27.5, 18.8. HRMS (ESI): m/z calcd for $C_{94}H_{98}N_{12}O_{12}$ $[M + 2H]^{2+}$: 794.3786, found: 794.3777. Melting point: 286.6 – 288.4 °C. Elemental Analysis: predicted: C, 71.10%; H, 6.22%; N, 10.59%; found: C, 70.96%; H, 6.23%; N, 10.70%.

UV-vis, fluorescence, and NMR studies

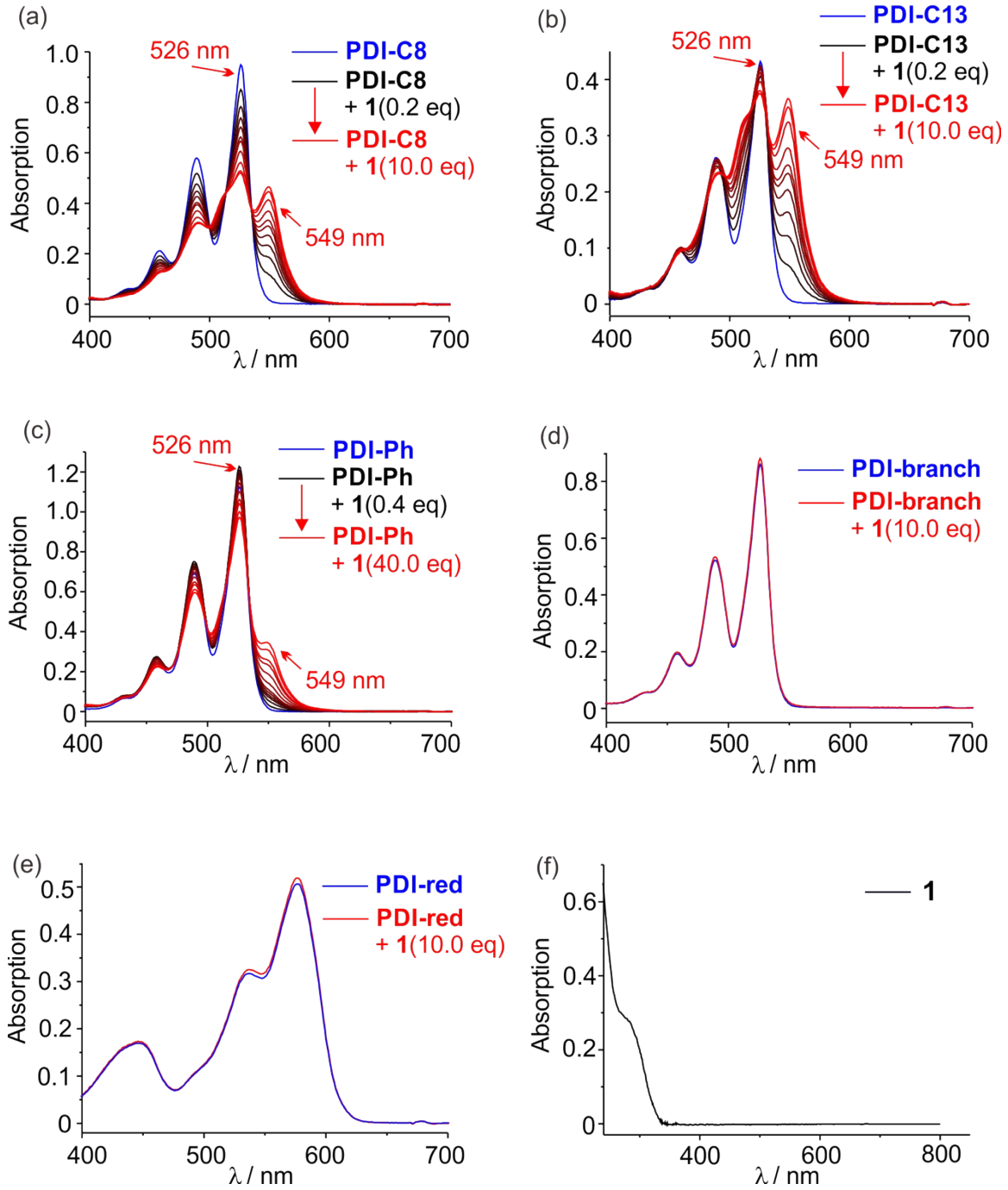

Figure S1. UV-vis titration study. (a) **PDI-C8** in $CHCl_3$ (80 μM, blue line) titrated with **1** ($CHCl_3$, 4 mM with 80 μM **PDI-C8**) from 0.2 to 10 equivalents (black to red lines). (b) **PDI-C13** in $CHCl_3$ (100 μM, blue line) titrated with **1** ($CHCl_3$, 4 mM with 100 μM **PDI-C13**) from 0.2 to 10 equivalents (black to red lines). (c) **PDI-Ph** in $CHCl_3$ (10 μM, blue line) titrated with **1** ($CHCl_3$, 4 mM with 10 μM **PDI-Ph**) from 0.4 to 40 equivalents (black to red lines). (d)

PDI-branch in $CHCl_3$ (100 μM, blue line) titrated with **1** ($CHCl_3$, 4 mM with 100 μM **PDI-branch**) up to 10 equivalents (red line). (e) **PDI-red** in $CHCl_3$ (100 μM, blue line) titrated with **1** ($CHCl_3$, 4 mM with 100 μM **PDI-red**) up to 10 equivalents (red line). (f) **1** in $CHCl_3$ (100 μM).

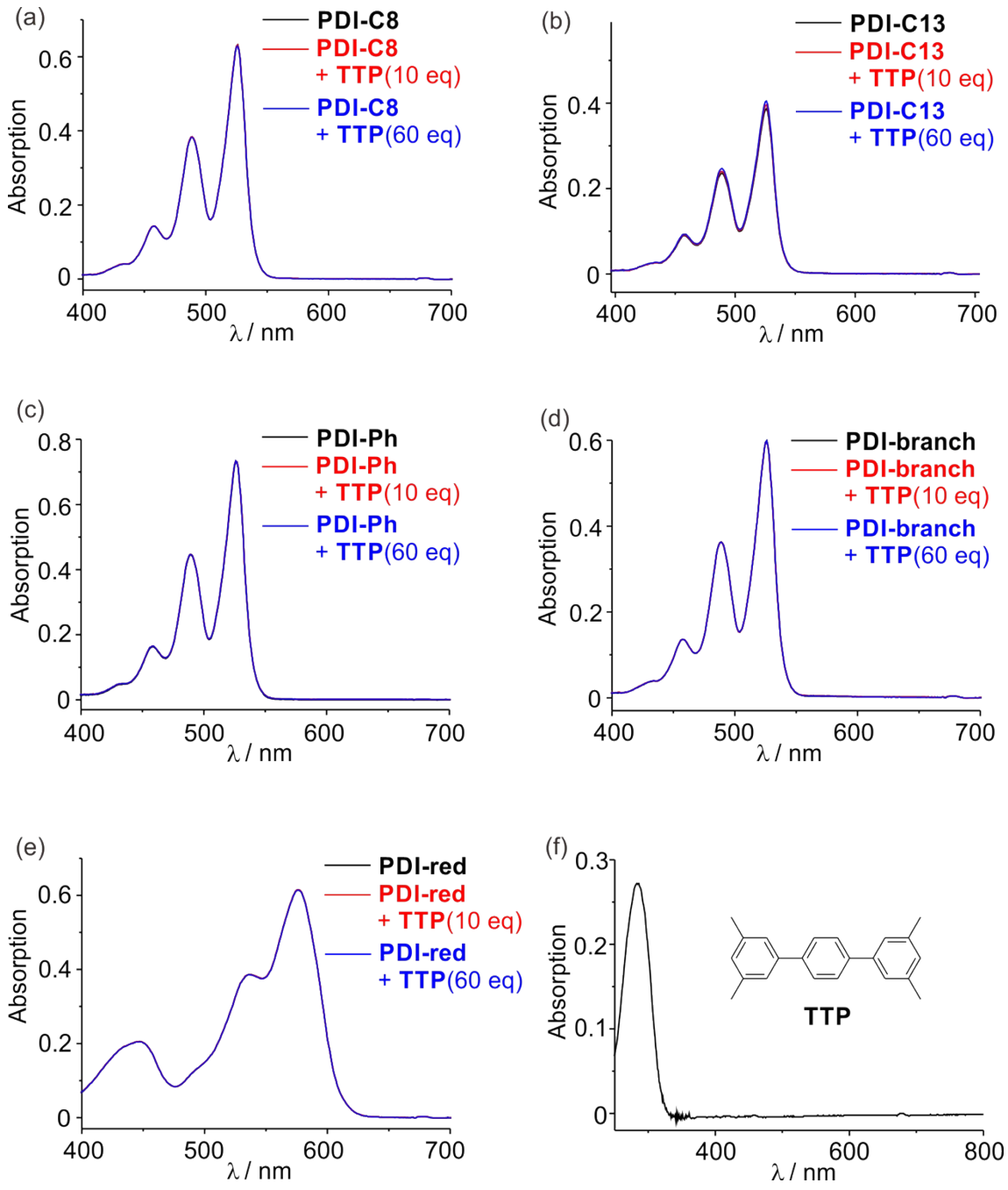

Figure S2. UV-vis titration study (control group with **TTP**). (a) **PDI-C8** in $CHCl_3$ (80 μM, black line) titrated with **TTP** (in $CHCl_3$, 40 mM with 80 μM **PDI-C8**) up to 10 (blue line) and 60 equivalents (red line). (b) **PDI-C13** in $CHCl_3$ (100 μM, black line) titrated with **TTP** (in $CHCl_3$, 40 mM with 100 μM **PDI-C13**) up to 10 (blue line) and 60 equivalents (red line). (c) **PDI-Ph** in $CHCl_3$ (10 μM, black line) titrated with **TTP** (in $CHCl_3$, 40 mM with 10 μM **PDI-Ph**) up to 10 (blue line) and 60 equivalents (red line). (d) **PDI-branch** in $CHCl_3$ (100 μM, black line) titrated with **TTP** (in $CHCl_3$, 40 mM with 100 μM **PDI-branch**) up to 10 (blue line) and 60 equivalents (red line). (e) **PDI-**

red in $CHCl_3$ (100 μM, black line) titrated with **TTP** (in $CHCl_3$, 40 mM with 100 μM **PDI-red**) up to 10 (blue line) and 60 equivalents (red line). (f) **TTP** in $CHCl_3$ (100 μM).

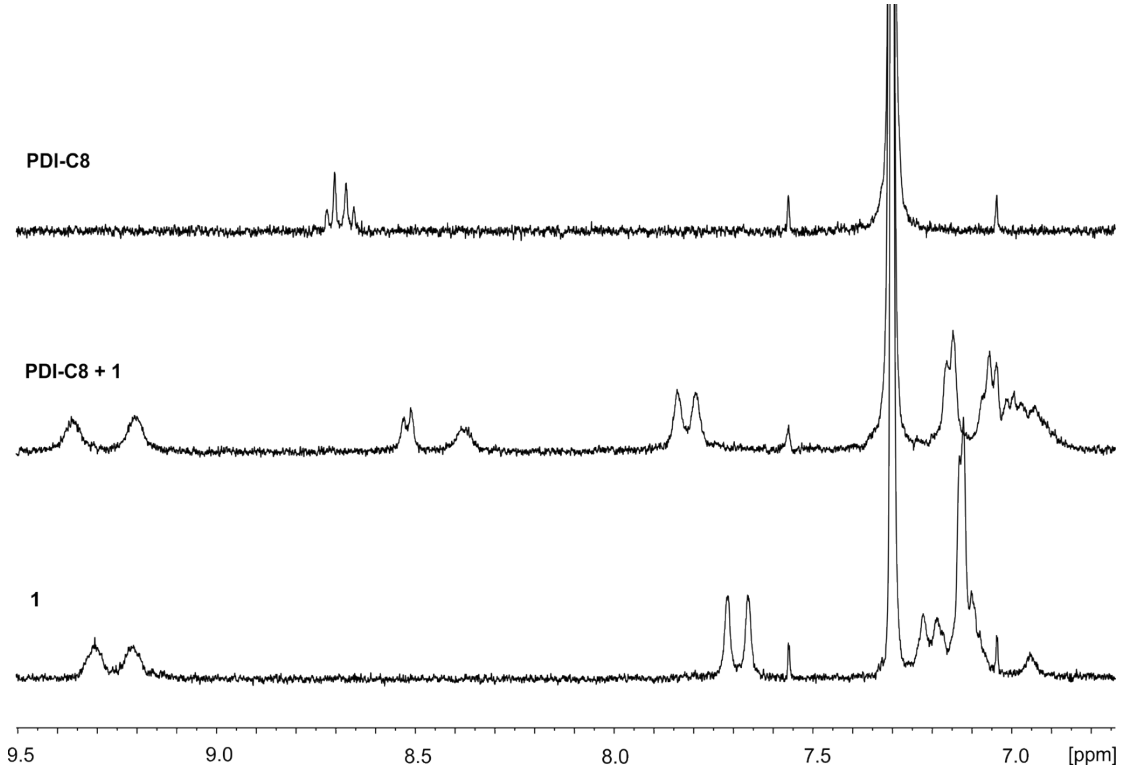

Figure S3. ^{1}H NMR (400 MHz, 298 K) spectra. From bottom to top, **1** in 2% DMSO-d_6/$CDCl_3$ (1 mM), **1** (1 mM) + **PDI-C8** (1 mM) in 2% DMSO-d_6/$CDCl_3$, and **PDI-C8** (1 mM) in 2% DMSO-d_6/$CDCl_3$.

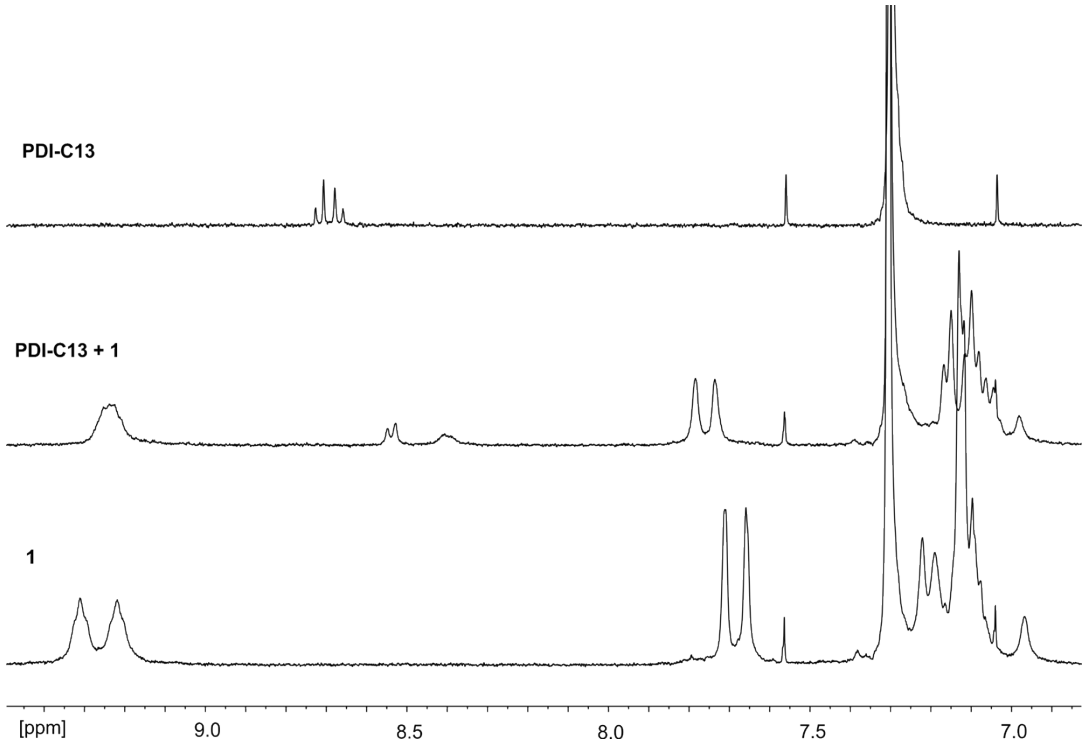

Figure S4. ^{1}H NMR (400 MHz, 298 K) spectra. From bottom to top, **1** in 2% DMSO-d_6/$CDCl_3$ (1.5 mM), **1** (1.5 mM) + **PDI-C13** (1 mM) in 2% DMSO-d_6/$CDCl_3$, and **PDI-C13** (1 mM) in 2% DMSO-d_6/$CDCl_3$.

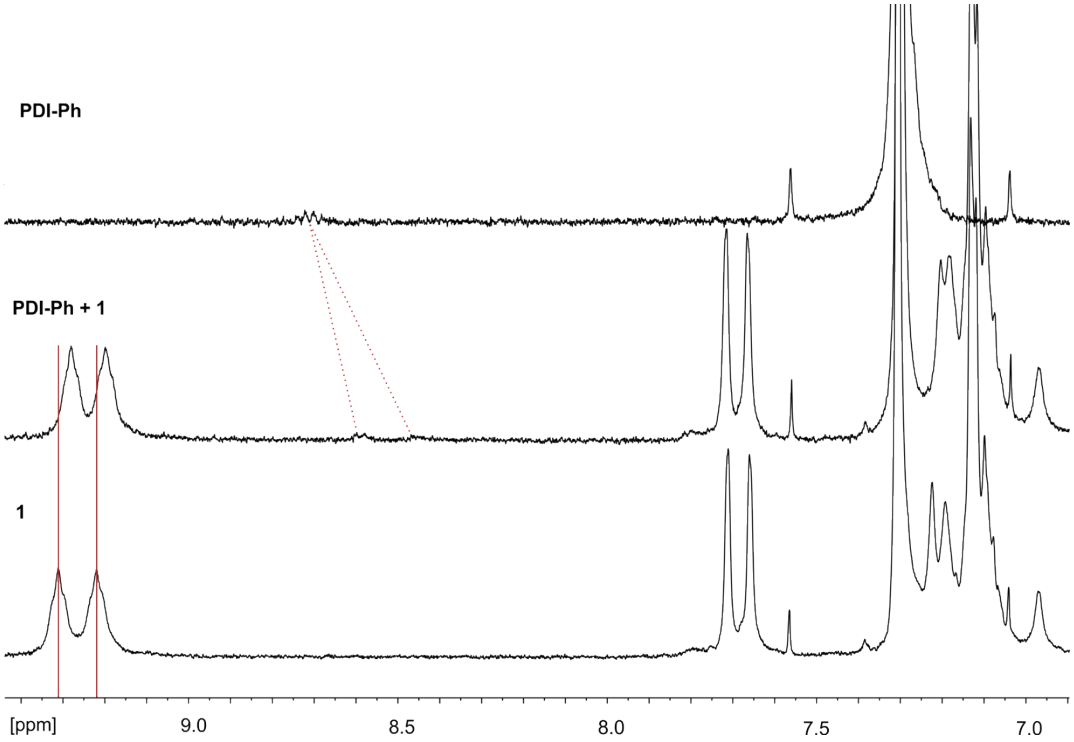

Figure S5. ^{1}H NMR (400 MHz, 298 K) spectra. From bottom to top, **1** in 2% DMSO-d_6/$CDCl_3$ (1.5 mM), **1** (1.5 mM) + **PDI-Ph** (0.2 mM) in 2% DMSO-d_6/$CDCl_3$, and **PDI-Ph** (0.2 mM) in 2% DMSO-d_6/$CDCl_3$. Chemical shifts of amide protons of **1** and perylene protons of **PDI-Ph** are indicated by red solid and dotted lines, respectively.

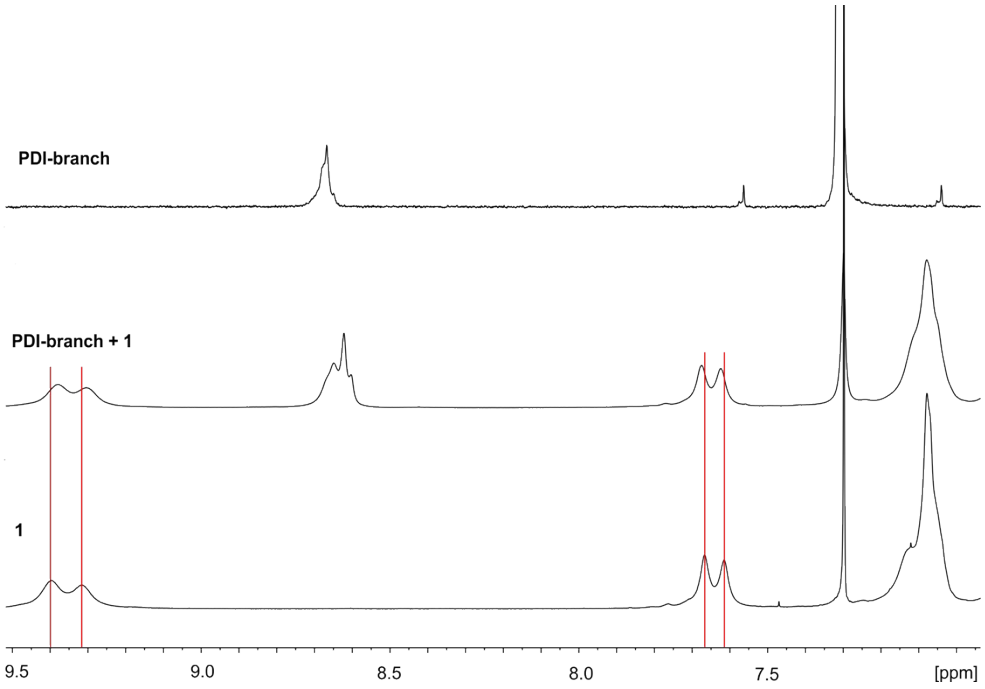

Figure S6. ^{1}H NMR (400 MHz, 298 K) spectra. From bottom to top, **1** in 2% DMSO-d_6/$CDCl_3$ (1.5 mM), **1** (1.5 mM) + **PDI-branch** (1.5 mM) in 2% DMSO-d_6/$CDCl_3$, and **PDI-branch** (1.5 mM) in 2% DMSO-d_6/$CDCl_3$. Chemical shifts of amide protons of **1** are indicated by red lines.

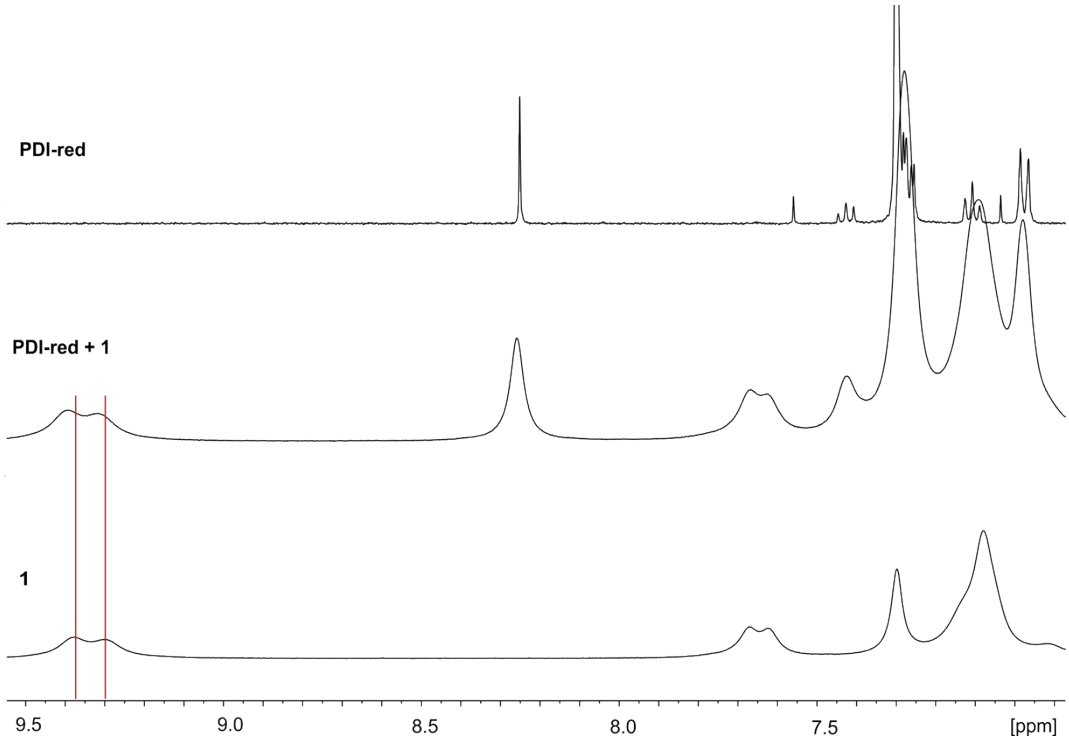

Figure S7. ^{1}H NMR (400 MHz, 298 K) spectra. From bottom to top, **1** in 2% DMSO-d_6/$CDCl_3$ (3 mM), **1** (3 mM) + **PDI-red** (3 mM) in 2% DMSO-d_6/$CDCl_3$, and **PDI-red** (1 mM) in 2% DMSO-d_6/$CDCl_3$. Chemical shifts of amide protons of **1** are indicated by red lines.

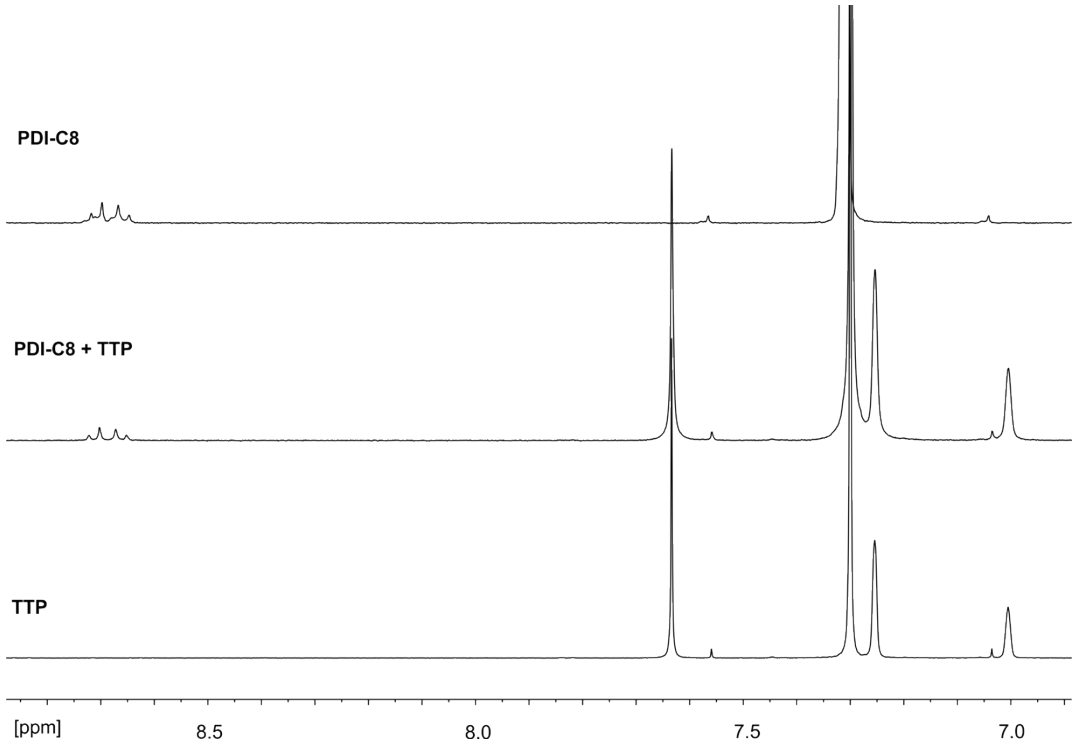

Figure S8. ^{1}H NMR (400 MHz, 298 K) spectra. From bottom to top, **TTP** in 2% DMSO-d_6/$CDCl_3$ (3 mM), **TTP** (3 mM) + **PDI-C8** (1 mM) in 2% DMSO-d_6/$CDCl_3$, and **PDI-C8** (1 mM) in 2% DMSO-d_6/$CDCl_3$.

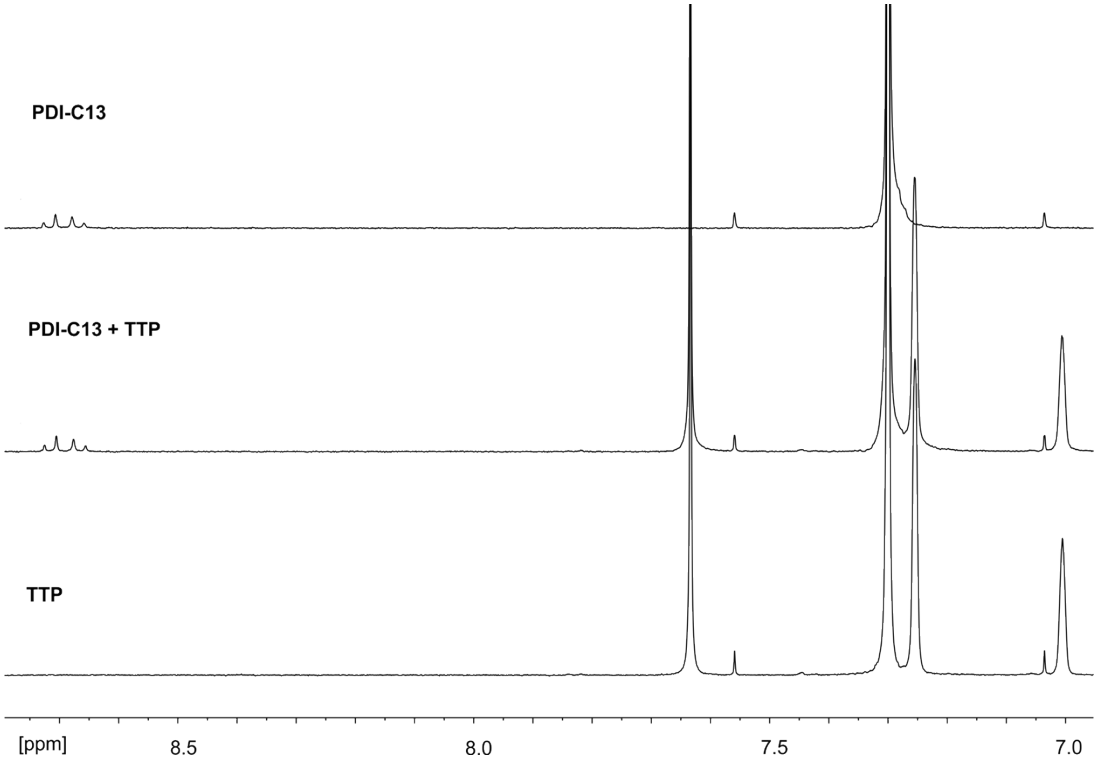

Figure S9. ^{1}H NMR (400 MHz, 298 K) spectra. From bottom to top, **TTP** in 2% DMSO-d_6/$CDCl_3$ (3 mM), **TTP** (3 mM) + **PDI-C13** (1 mM) in 2% DMSO-d_6/$CDCl_3$, and **PDI-C13** (1 mM) in 2% DMSO-d_6/$CDCl_3$.

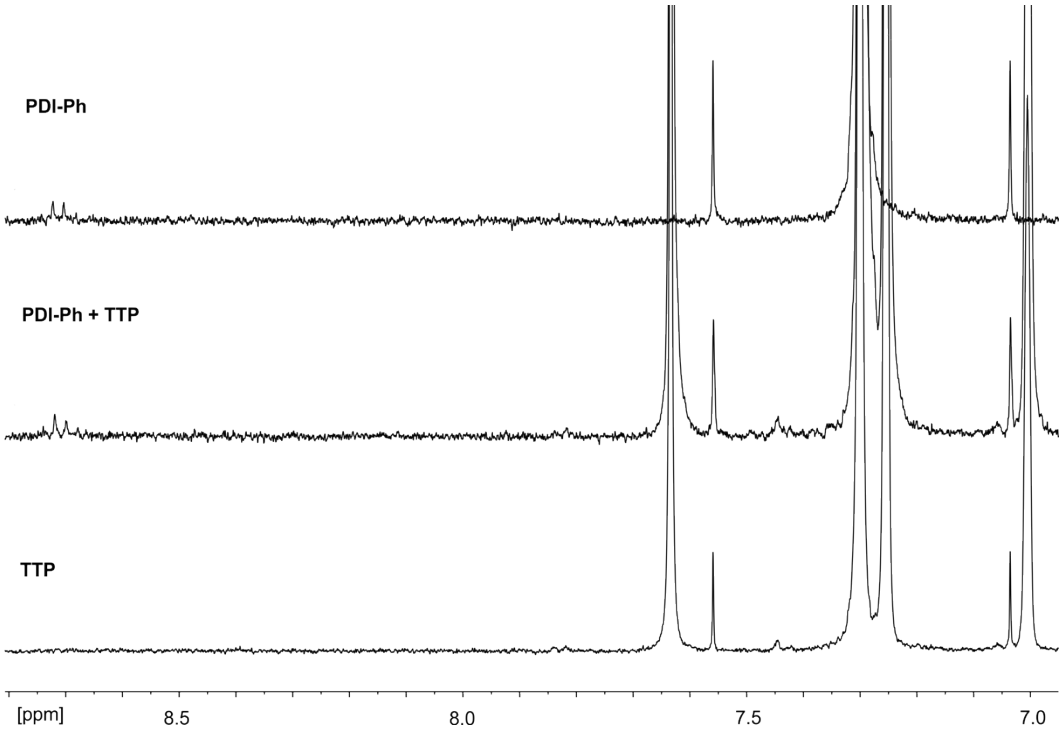

Figure S10. ^{1}H NMR (400 MHz, 298 K) spectra. From bottom to top, **TTP** in 2% DMSO-d_6/$CDCl_3$ (3 mM), **TTP** (3 mM) + **PDI-Ph** (0.2 mM) in 2% DMSO-d_6/$CDCl_3$, and **PDI-Ph** (0.2 mM) in 2% DMSO-d_6/$CDCl_3$.

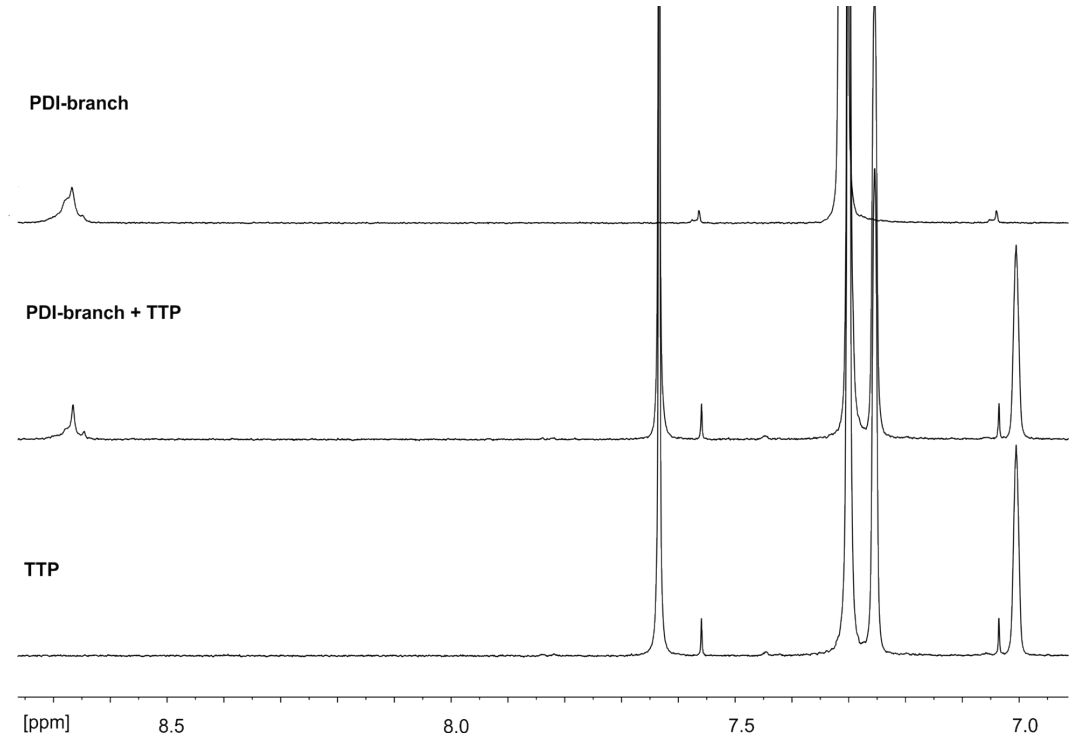

Figure S11. ^{1}H NMR (400 MHz, 298 K) spectra. From bottom to top, **TTP** in 2% DMSO-d_6/$CDCl_3$ (3 mM), **TTP** (3 mM) + **PDI-branch** (1.5 mM) in 2% DMSO-d_6/$CDCl_3$, and **PDI-branch** (1.5 mM) in 2% DMSO-d_6/$CDCl_3$.

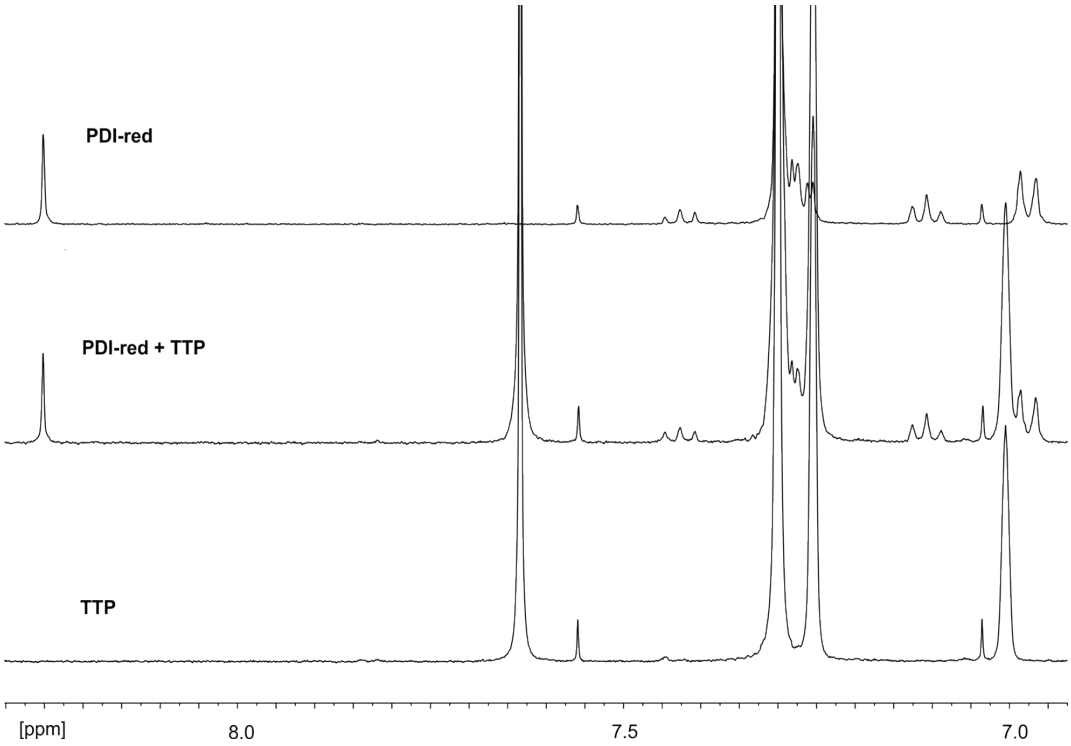

Figure S12. ^{1}H NMR (400 MHz, 298 K) spectra. From bottom to top, **TTP** in 2% DMSO-d_6/$CDCl_3$ (3 mM), **TTP** (3 mM) + **PDI-red** (1 mM) in 2% DMSO-d_6/$CDCl_3$, and **PDI-red** (1 mM) in 2% DMSO-d_6/$CDCl_3$.

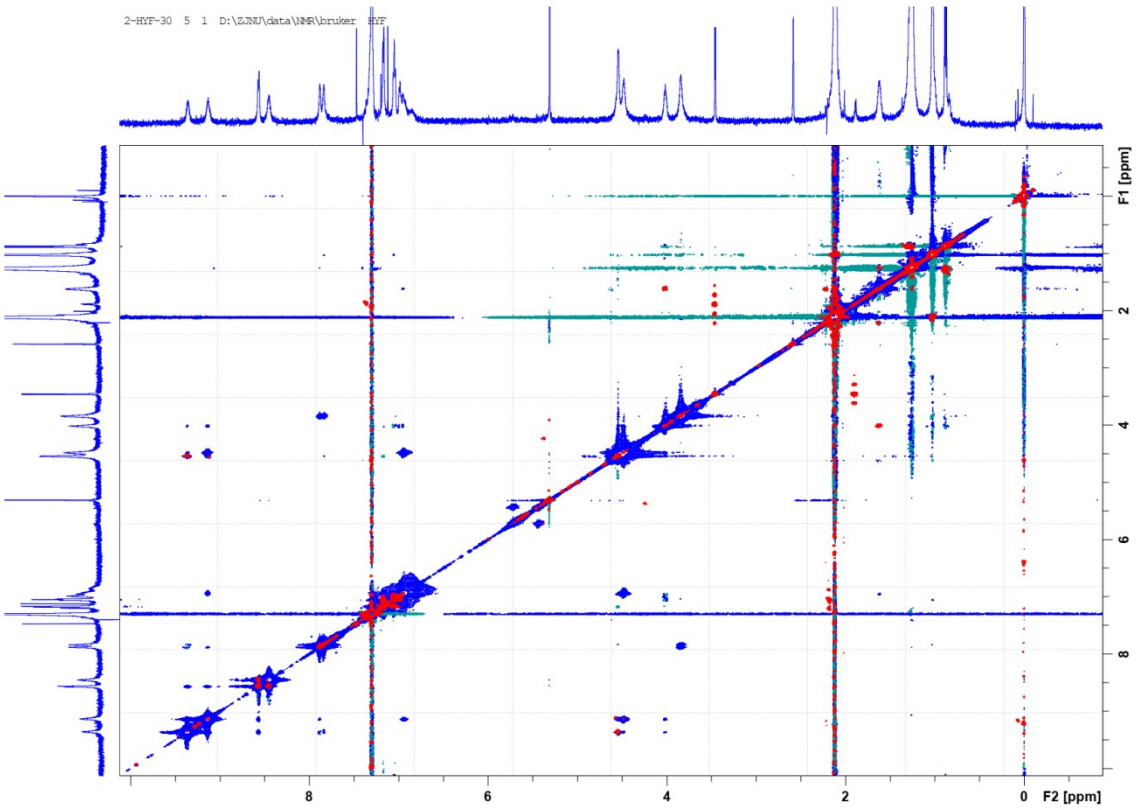

Figure S13. Full ^{1}H-^{1}H NOESY (600 MHz blue) and ^{1}H-^{1}H COSY (600 MHz red) overlapped spectra of **1** (1 mM) + **PDI-C8** (1.2 mM) in 2% DMSO-d_6/$CDCl_3$ at 298 K.

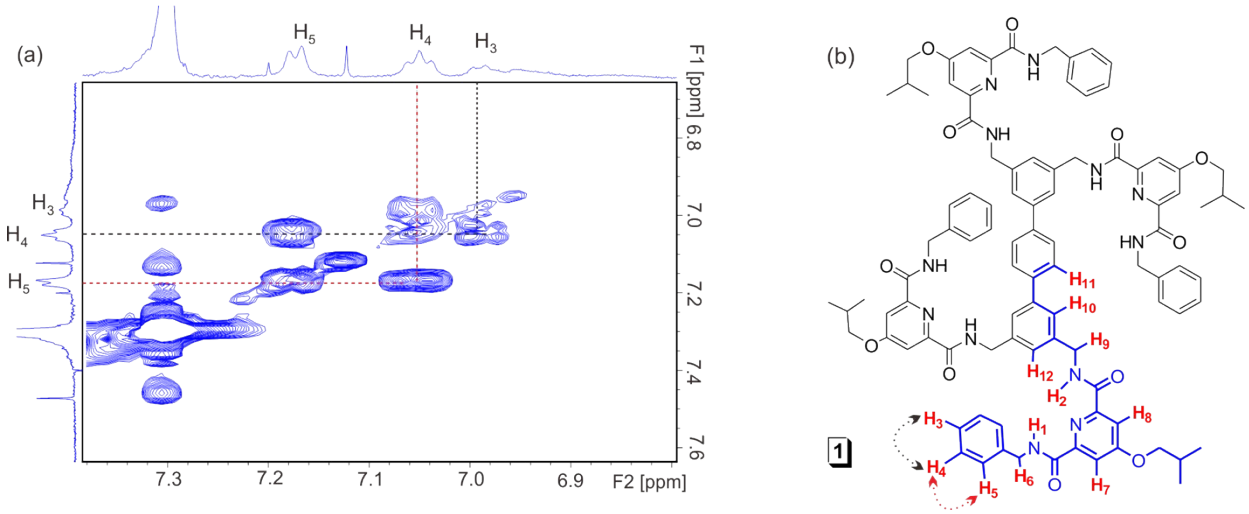

Figure S14. (a) ^{1}H-^{1}H COSY (600 MHz) spectrum of **1** (1 mM) + **PDI-C8** (1.2 mM) in 2% DMSO-d_6/$CDCl_3$ at 298 K, showing $H_3 \leftrightarrow H_4$ and $H_4 \leftrightarrow H_5$ correlations. (b) shows a quarter of the corresponding correlations in the structure of **1**.

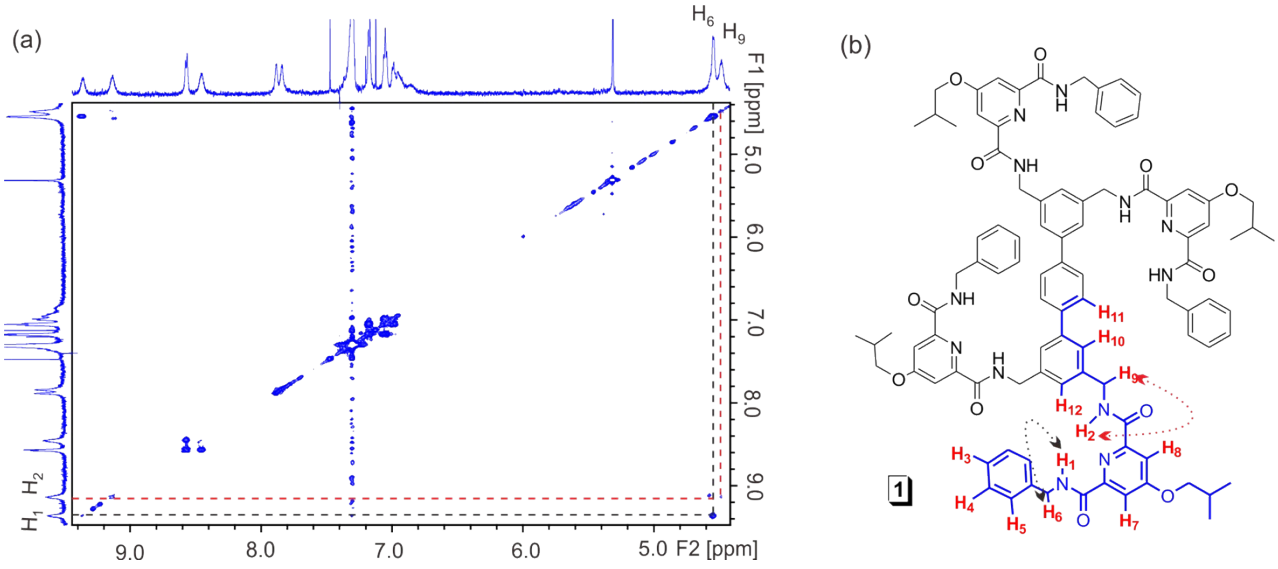

Figure S15. (a) ^{1}H-^{1}H COSY (600 MHz) spectrum of **1** (1 mM) + **PDI-C8** (1.2 mM) in 2% DMSO-d_6/$CDCl_3$ at 298 K, showing $H_1 \leftrightarrow H_6$ and $H_2 \leftrightarrow H_9$ correlations. (b) shows a quarter of the corresponding correlations in the structure of **1**.

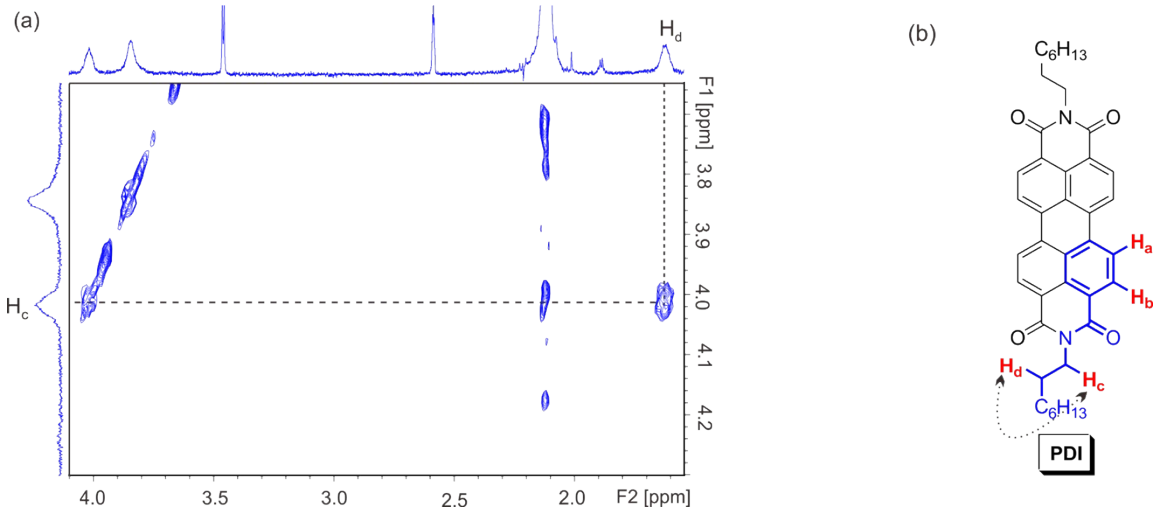

Figure S16. (a) ^{1}H-^{1}H COSY (600 MHz) spectrum of **1** (1 mM) + **PDI-C8** (1.2 mM) in 2% DMSO-d_6/$CDCl_3$ at 298 K, showing the $H_d \leftrightarrow H_c$ correlation. (b) shows a quarter of the corresponding correlations in the structure of **PDI-C8**.

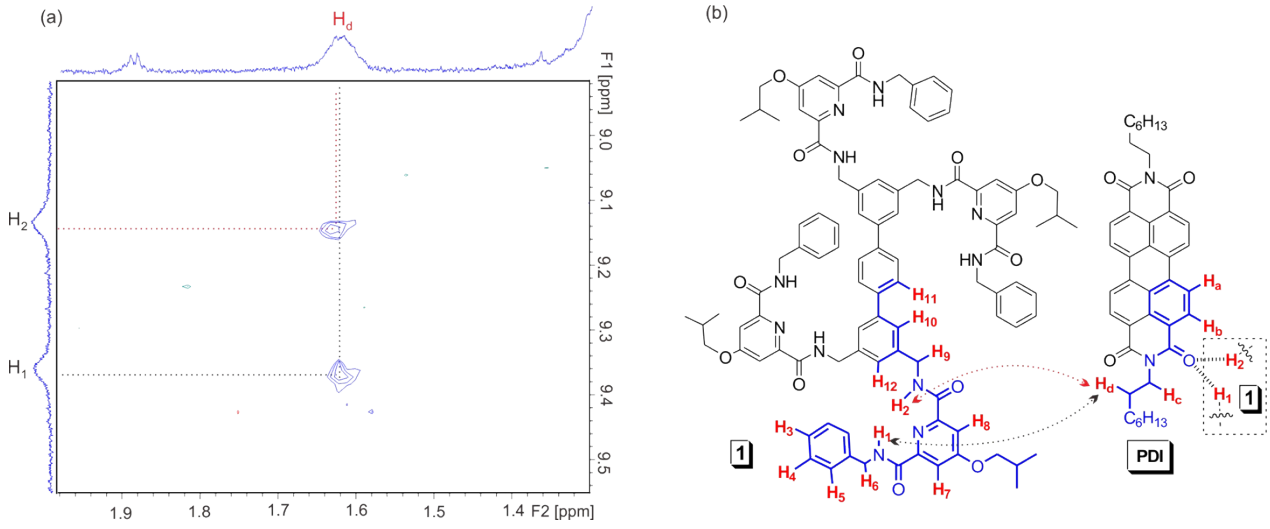

Figure S17. (a) ^{1}H-^{1}H NOESY (600 MHz) spectrum of **1** (1 mM) + **PDI-C8** (1.2 mM) in 2% DMSO-d_6/$CDCl_3$ at 298 K, showing $H_1 \leftrightarrow H_d$ and $H_2 \leftrightarrow H_d$ correlations. (b) shows a quarter of the corresponding correlations in the structures of **1** and **PDI-C8**.

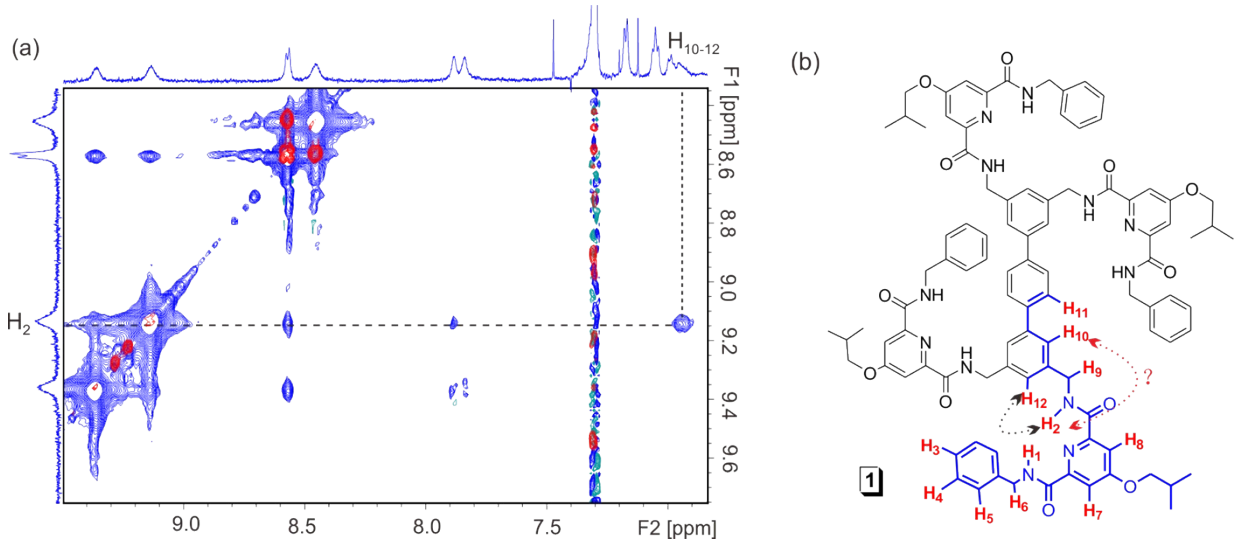

Figure S18. (a) ^{1}H-^{1}H NOESY (600 MHz) spectrum of **1** (1 mM) + **PDI-C8** (1.2 mM) in 2% DMSO-d_6/$CDCl_3$ at 298 K, showing $H_{12} \leftrightarrow H_2$ and $H_2 \leftrightarrow H_{10}$ correlations.. (b) shows a quarter of the corresponding correlations in structure of **1**.

Table S1. Selected NOE correlations and the corresponding distances in the **PDI-C8⊂1** complex.

ROE correlations[a]	**F2 (ppm)**	**F1 (ppm)**	**Distances r_{ij}(Å)**[b]
$H_b \leftrightarrow H_1$	9.37	8.57	3.49
$H_b \leftrightarrow H_2$	9.14	8.57	3.62
$H_c \leftrightarrow H_1$	9.37	4.02	4.56
$H_c \leftrightarrow H_2$	9.14	4.02	4.02
$H_d \leftrightarrow H_1$	9.37	1.62	4.81
$H_d \leftrightarrow H_2$	9.14	1.62	4.99
$H_2 \leftrightarrow H_1$	9.37	9.14	2.92
Reference ($H_4 \leftrightarrow H_5$)	7.17	7.05	2.48[c]

[a] Selected from ^{1}H-^{1}H NOESY spectrum (600 MHz, 298 K) of **1** (1 mM) + **PDI-C8** (1.2 mM) in 2% DMSO-d_6/$CDCl_3$. [b] Calculated using the equation[4]: $r_{ij} = r_{ref}\left(\frac{a_{ref}}{a_{ij}}\right)^{1/6}$. [c] An approximate value from a molecular model of **1** optimized by MacroModel (Schrödinger Inc.) via MMFFs.

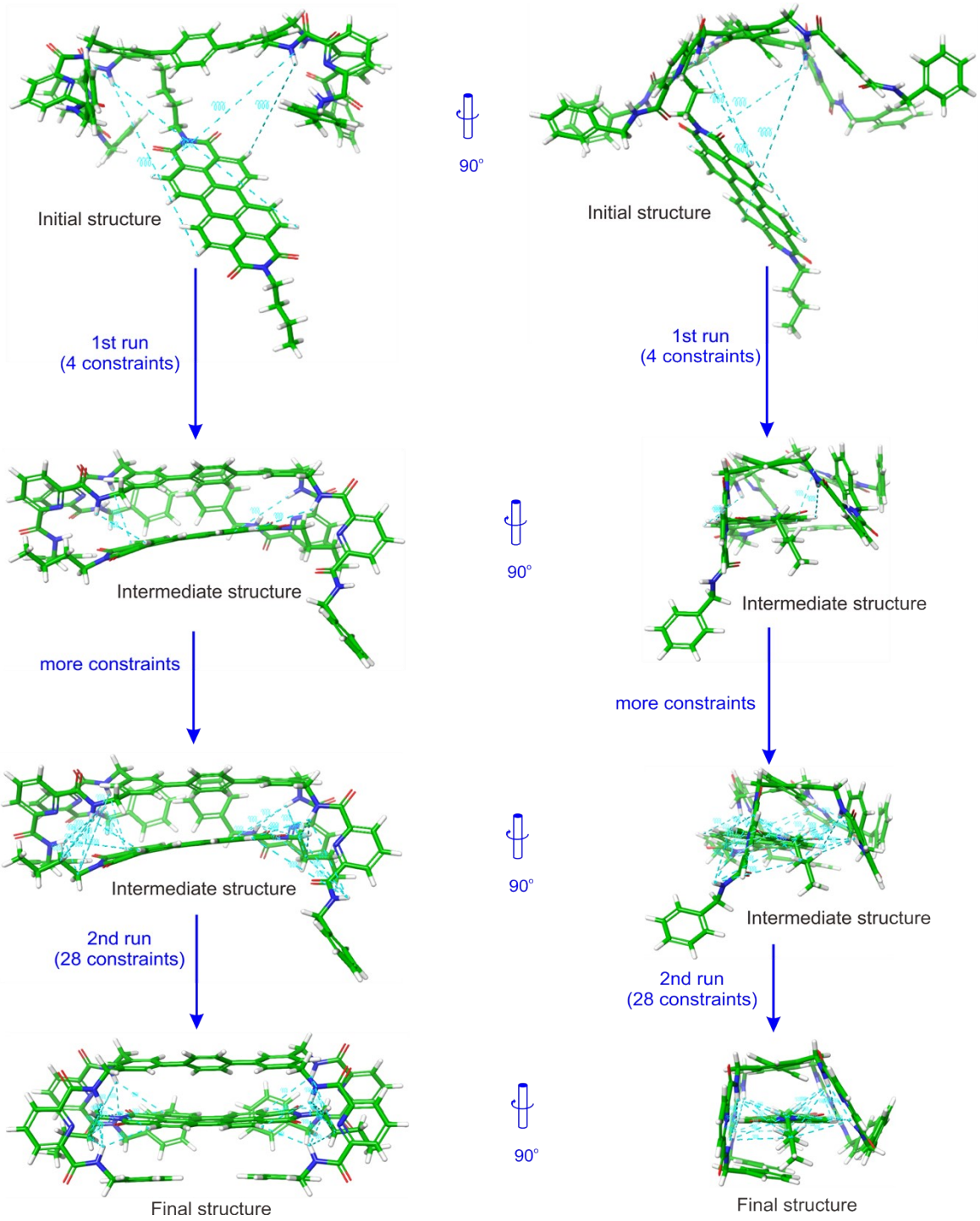

Figure S19. Molecular modeling of the **PDI-C8⊂1** complex with distance constraints (obtained from NOE correlations, Table S1) by MacroModel (Schrödinger Inc.) via MMFFs. From top to bottom, the starting opened and separated structures (initial structure), the preliminary host-guest recognized structures (intermediate structure) after putting 4 distance constraints ($H_2 \leftrightarrow H_b$ correlations), the intermediate structure with 28 distance constraints, and the resulting **PDI-C8⊂1** complex structure (final structure). Distance constraints are shown in blue dashed lines. C, O, N, and H atoms are shown in green, red, blue and white, respectively. Redundant side chains are omitted for clarity.

Figure S20. Overlapped 20 NMR simulated structures showing structural vibration of the **PDI-C8⊂1** complex (**PDI-C8** in red and **1** in green). The other 19 structures were obtained by repeating the process in figure S19 for 19 times with different initial structures.

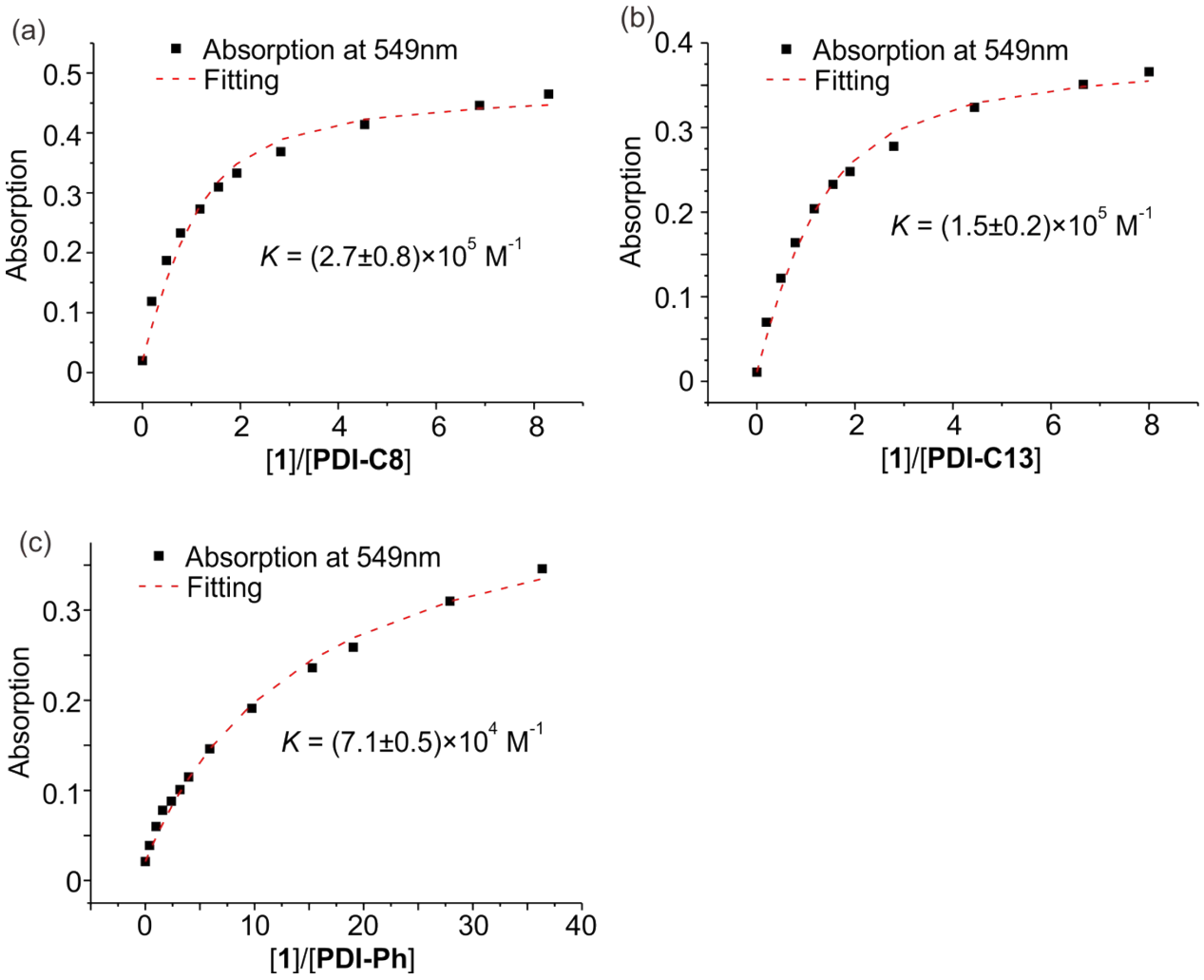

Figure S21. Binding analysis curve of the UV-vis titration study in figure S1 (the absorption changes at 549 nm were analyzed). (a) **PDI-C8** + **1** in $CHCl_3$, giving binding constant $K = (2.7 \pm 0.8) \times 10^5$ M^{-1}. (b) **PDI-C13** + **1** in $CHCl_3$, giving binding constant $K = (1.5 \pm 0.2) \times 10^5$ M^{-1}. (c) **PDI-Ph** + **1** in $CHCl_3$, giving binding constant $K = (7.1 \pm 0.5) \times 10^4$ M^{-1}. The data were fitted using a 1:1 receptor-substrate binding model via an excellent binding analysis website "http://supramolecular.org/".[5]

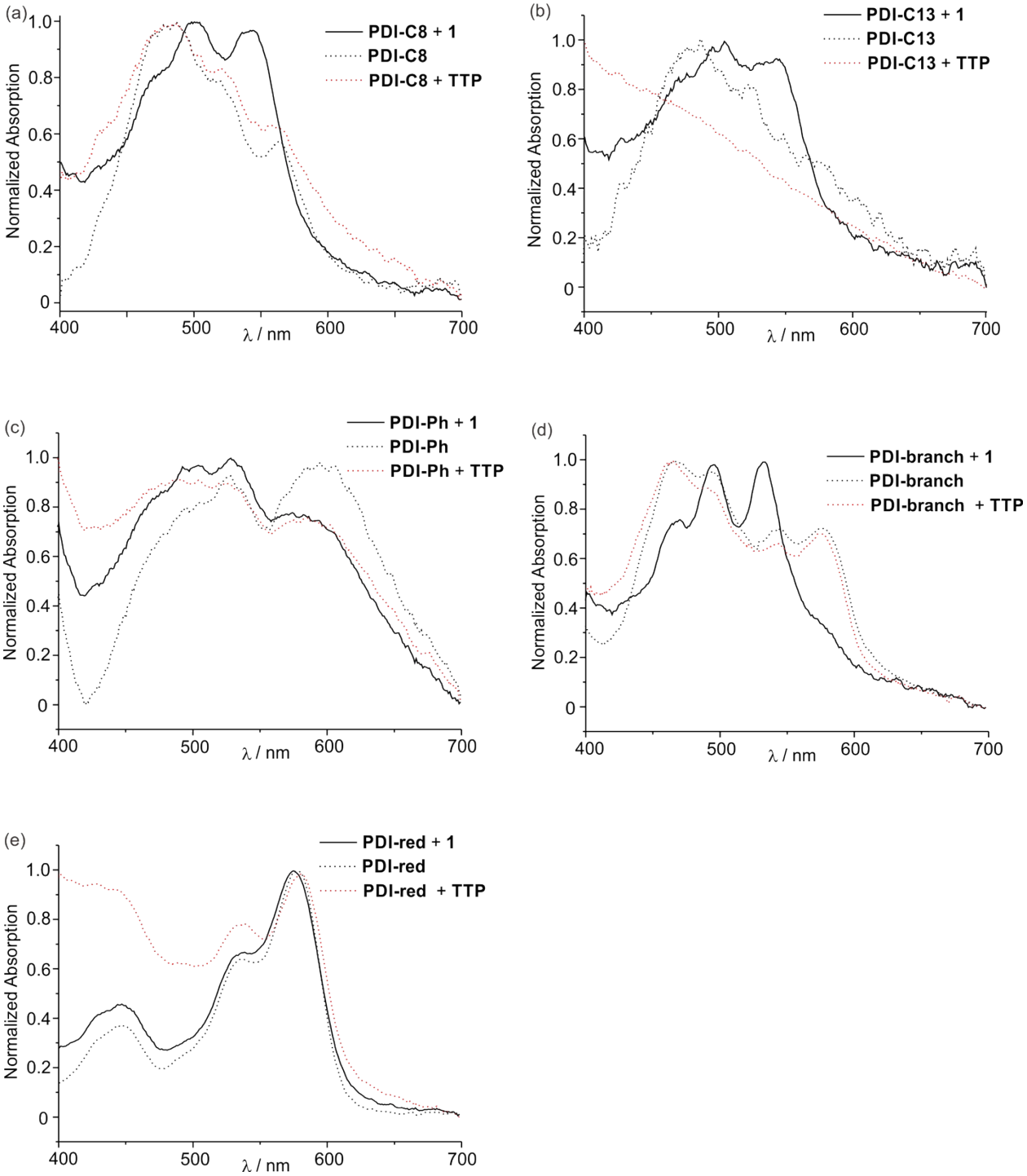

Figure S22. Normalized UV-vis spectra of film samples. (a) **PDI-C8**+**1** (black line), **PDI-C8** (black dotted line), **PDI-C8**+**TTP** (red dotted line). (b) **PDI-C13**+**1** (black line), **PDI-C13** (black dotted line), **PDI-C13**+**TTP** (red dotted line). (c) **PDI-Ph**+**1** (black line), **PDI-Ph** (black dotted line), **PDI-Ph** +**TTP** (red dotted line). (d) **PDI-branch**+**1** (black line), **PDI-branch** (black dotted line), **PDI-branch**+**TTP** (red dotted line). (e) **PDI-red**+**1** (black line), **PDI-red** (black dotted line), **PDI-red**+**TTP** (red dotted line). The molar ratio of PDI to **1** is 1 : 1 while PDI to **TTP** is 1 : 5.5 (equivalent to the weight ratio of PDI to **1**).

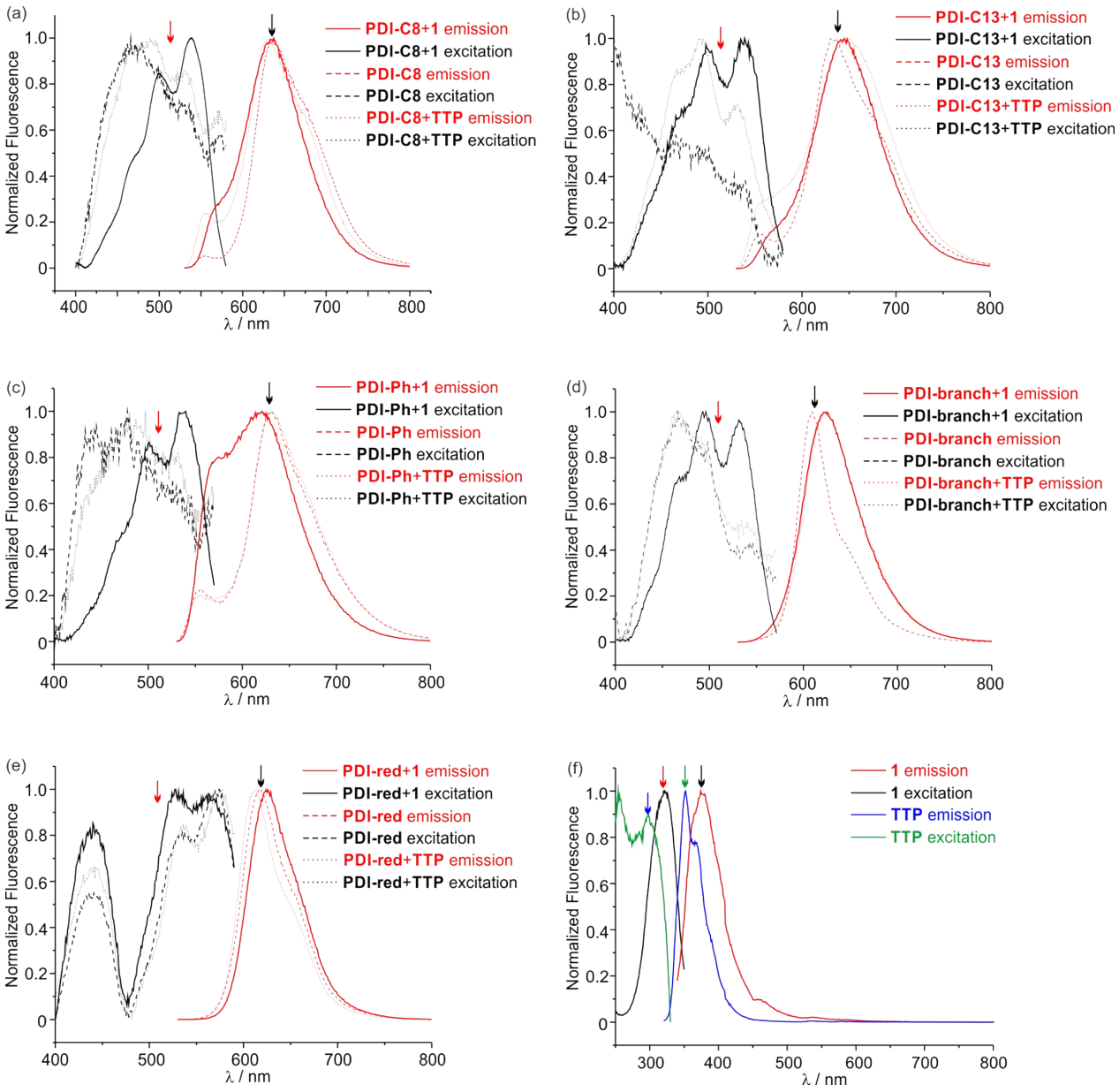

Figure S23. Normalized fluorescence spectra of (a) **PDI-C8**, **PDI-C8** + **1**, and **PDI-C8** + **TTP**; (b) **PDI-C13**, **PDI-C13** + **1**, and **PDI-C13** + **TTP**; (c) **PDI-Ph**, **PDI-Ph** + **1**, and **PDI-Ph** + **TTP**; (d) **PDI-branch**, **PDI-branch** + **1**, and **PDI-branch** + **TTP**; (e) **PDI-red**, **PDI-red** + **1**, and **PDI-red** + **TTP** (f) **1** and **TTP** in film form. The molar ratio of PDI to **1** is 1 : 1 while PDI to **TTP** is 1 : 5.5 (equivalent to the weight ratio of PDI to **1**); colored arrows indicate excitation or emission points of the corresponding emission or excitation spectra.

Table S2. Summary of fluorescence lifetimes.

	PDI (in solid)		PDI + **1** (in solid)		PDI + **TTP** (in solid)		PDI (in $CHCl_3$)	
	Lifetime (τ) / ns	Average lifetime (τ)/ ns	Lifetime (τ) / ns	Average lifetime (τ)/ ns	Lifetime (τ) / ns	Average lifetime (τ)/ ns	Lifetime (τ) / ns	Average lifetime (τ)/ ns
PDI-C8 (film)	$\tau_1 = 1.2$ (91.73%) $\tau_2 = 4.0$ (8.27%) $\chi^2 = 1.254$	$\tau_{avg} = 1.4$	$\tau_1 = 2.2$ (40.63%) $\tau_2 = 10.5$ (26.75%) $\tau_3 = 23.3$ (32.62%) $\chi^2 = 0.969$	$\tau_{avg} = 11.3$	$\tau_1 = 0.8$ (41.18%) $\tau_2 = 2.1$ (54.92%) $\tau_3 = 7.0$ (3.90%) $\chi^2 = 1.051$	$\tau_{avg} = 1.7$	$\tau_1 = 4.4$ (99.24%) $\tau_2 = 21.0$ (0.76%) $\chi^2 = 1.155$	$\tau_{avg} = 4.5$
PDI-C8 (Powder)	- [a]	- [a]	$\tau_1 = 1.4$ (28.96%) $\tau_2 = 4.2$ (51.97%) $\tau_3 = 16.3$ (19.07%) $\chi^2 = 1.267$	$\tau_{avg} = 5.7$	$\tau_1 = 0.8$ (92.59%) $\tau_2 = 3.8$ (7.41%) $\chi^2 = 0.940$	$\tau_{avg} = 1.0$		
PDI-C13 (film)	$\tau_1 = 0.5$ (58.81%) $\tau_2 = 1.8$ (35.24%) $\tau_3 = 5.4$ (5.95%) $\chi^2 = 1.015$	$\tau_{avg} = 1.2$	$\tau_1 = 1.7$ (74.42%) $\tau_2 = 5.3$ (17.77%) $\tau_3 = 15.9$ (7.51%) $\chi^2 = 0.910$	$\tau_{avg} = 3.4$	$\tau_1 = 0.6$ (72.00%) $\tau_2 = 2.1$ (24.75%) $\tau_3 = 7.0$ (3.26%) $\chi^2 = 0.901$	$\tau_{avg} = 1.2$	$\tau_1 = 0.4$ (25.04%) $\tau_2 = 4.6$ (74.96%) $\chi^2 = 1.088$	$\tau_{avg} = 3.6$
PDI-C13 (Powder)	$\tau_1 = 0.3$ (76.15%) $\tau_2 = 2.8$ (18.14%) $\tau_3 = 13.9$ (5.72%) $\chi^2 = 1.294$	$\tau_{avg} = 1.5$	$\tau_1 = 1.2$ (42.20%) $\tau_2 = 4.0$ (42.59%) $\tau_3 = 15.6$ (15.21%) $\chi^2 = 1.062$	$\tau_{avg} = 4.6$	$\tau_1 = 0.3$ (81.36%) $\tau_2 = 2.9$ (13.40%) $\tau_3 = 12.8$ (5.24%) $\chi^2 = 1.203$	$\tau_{avg} = 1.3$		
PDI-Ph (film)	- [a]	- [a]	$\tau_1 = 0.4$ (65.83%) $\tau_2 = 2.6$ (18.69%) $\tau_3 = 11.7$ (15.48%) $\chi^2 = 1.075$	$\tau_{avg} = 2.5$	- [a]	- [a]	$\tau_1 = 1.2$ (94.9%) $\tau_2 = 5.1$ (5.1%) $\chi^2 = 1.075$	$\tau_{avg} = 1.4$
PDI-Ph (Powder)	- [a]	- [a]	$\tau_1 = 0.8$ (72.14%)	$\tau_{avg} = 2.4$	- [a]	- [a]		

			$\tau_2 = 3.5$ (19.22%) $\tau_3 = 12.7$ (8.64%) $\chi^2 = 1.222$					
PDI-branch (film)	$\tau_1 = 1.0$ (59.91%) $\tau_2 = 2.1$ (35.20%) $\tau_3 = 6.8$ (4.89%) $\chi^2 = 1.094$	$\tau_{avg} = 1.7$	$\tau_1 = 3.6$ (4.12%) $\tau_2 = 16.7$ (43.94%) $\tau_3 = 28.4$ (51.94%) $\chi^2 = 1.115$	$\tau_{avg} = 22.2$	$\tau_1 = 0.9$ (55.25%) $\tau_2 = 2.4$ (34.74%) $\tau_3 = 6.6$ (10.02%) $\chi^2 = 1.203$	$\tau_{avg} = 2.0$	$\tau_1 = 4.8$ (100%) $\chi^2 = 1.247$	$\tau_{avg} = 4.8$
PDI-branch (Powder)	$\tau_1 = 0.7$ (41.54%) $\tau_2 = 2.6$ (38.12%) $\tau_3 = 6.5$ (20.34%) $\chi^2 = 1.114$	$\tau_{avg} = 2.6$	$\tau_1 = 2.9$ (11.68%) $\tau_2 = 12.2$ (47.61%) $\tau_3 = 28.4$ (40.71%) $\chi^2 = 1.151$	$\tau_{avg} = 17.7$	$\tau_1 = 0.8$ (52.99%) $\tau_2 = 2.9$ (39.47%) $\tau_3 = 7.4$ (7.54%) $\chi^2 = 1.244$	$\tau_{avg} = 2.1$		
PDI-red (film)	$\tau_1 = 0.7$ (96.70%) $\tau_2 = 5.8$ (3.30%) $\chi^2 = 1.074$	$\tau_{avg} = 0.9$	$\tau_1 = 3.2$ (53.12%) $\tau_2 = 7.1$ (42.67%) $\tau_3 = 31.3$ (4.22%) $\chi^2 = 1.162$	$\tau_{avg} = 6.0$	$\tau_1 = 1.4$ (74.90%) $\tau_2 = 3.2$ (22.81%) $\tau_3 = 12.3$ (2.30%) $\chi^2 = 1.146$	$\tau_{avg} = 2.0$	$\tau_1 = 0.1$ (13.7%) $\tau_2 = 6.8$ (86.3%) $\chi^2 = 1.173$	$\tau_{avg} = 5.8$
PDI-red (Powder)	$\tau_1 = 1.2$ (80.57%) $\tau_2 = 3.2$ (19.43%) $\chi^2 = 0.878$	$\tau_{avg} = 1.5$	$\tau_1 = 2.2$ (36.15%) $\tau_2 = 6.1$ (54.92%) $\tau_3 = 22.9$ (8.93%) $\chi^2 = 1.249$	$\tau_{avg} = 6.2$	$\tau_1 = 1.1$ (83.47%) $\tau_2 = 4.3$ (16.53%) $\chi^2 = 1.026$	$\tau_{avg} = 1.6$		

[a] Fluorescence is too low to obtain the corresponding fluorescence lifetime.

Table S3. Summary of quantum yields in film form.

quantum yield Φ (%)	PDI	PDI + **1**	PDI + Me-β-CD	PDI + γ-CD	PDI + CB[8]
PDI-C8	3.1	28.5	1.1	2.2	1.6
PDI-C13	2.9	13.0	2.3	1.8	1.4
PDI-Ph	-[a]	1.5	-[a]	-[a]	-[a]
PDI-branch	3.4	58.5	10.9	3.4	6.7
PDI-red	18.6	55.4	14.5	10.2	13.6

[a] Quantum yield is too low to be determined.

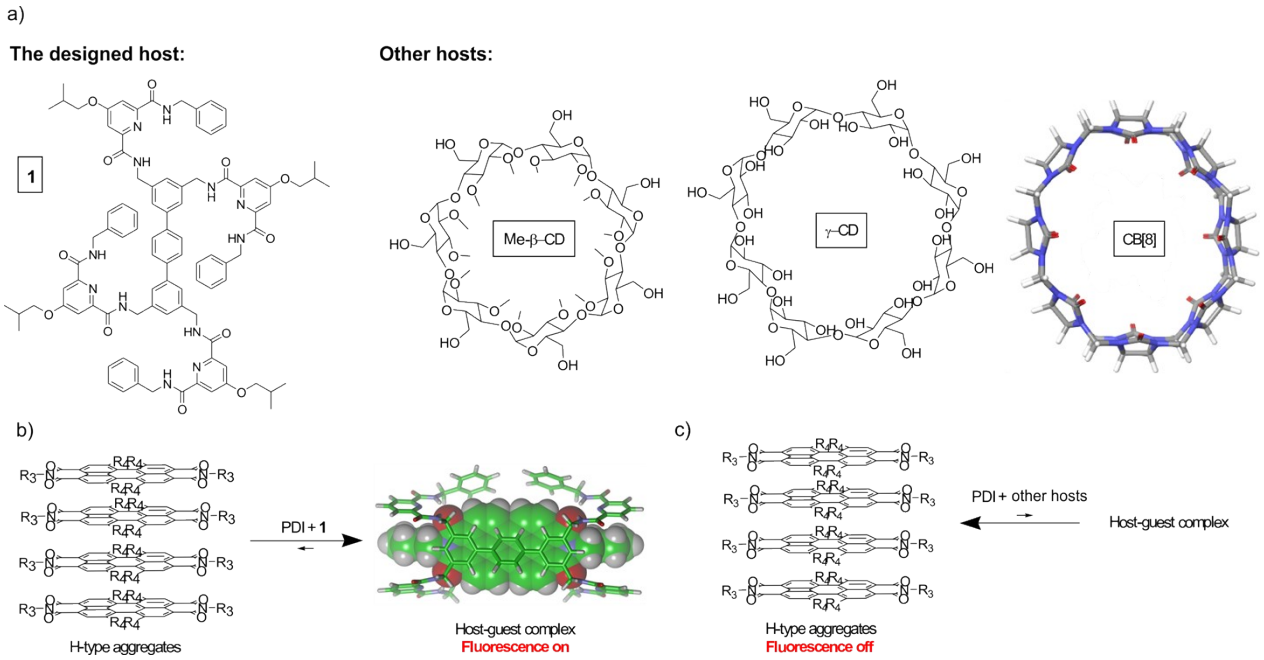

Figure S24. (a) Structures of the designed host **1** and other hosts, Me-β-CD, γ-CD, and CB[8]. (b) PDI + **1** give host-guest complexes, fluorescence on states. (c) PDI + other hosts yield H-type aggregates of PDI dyes, fluorescence off states.

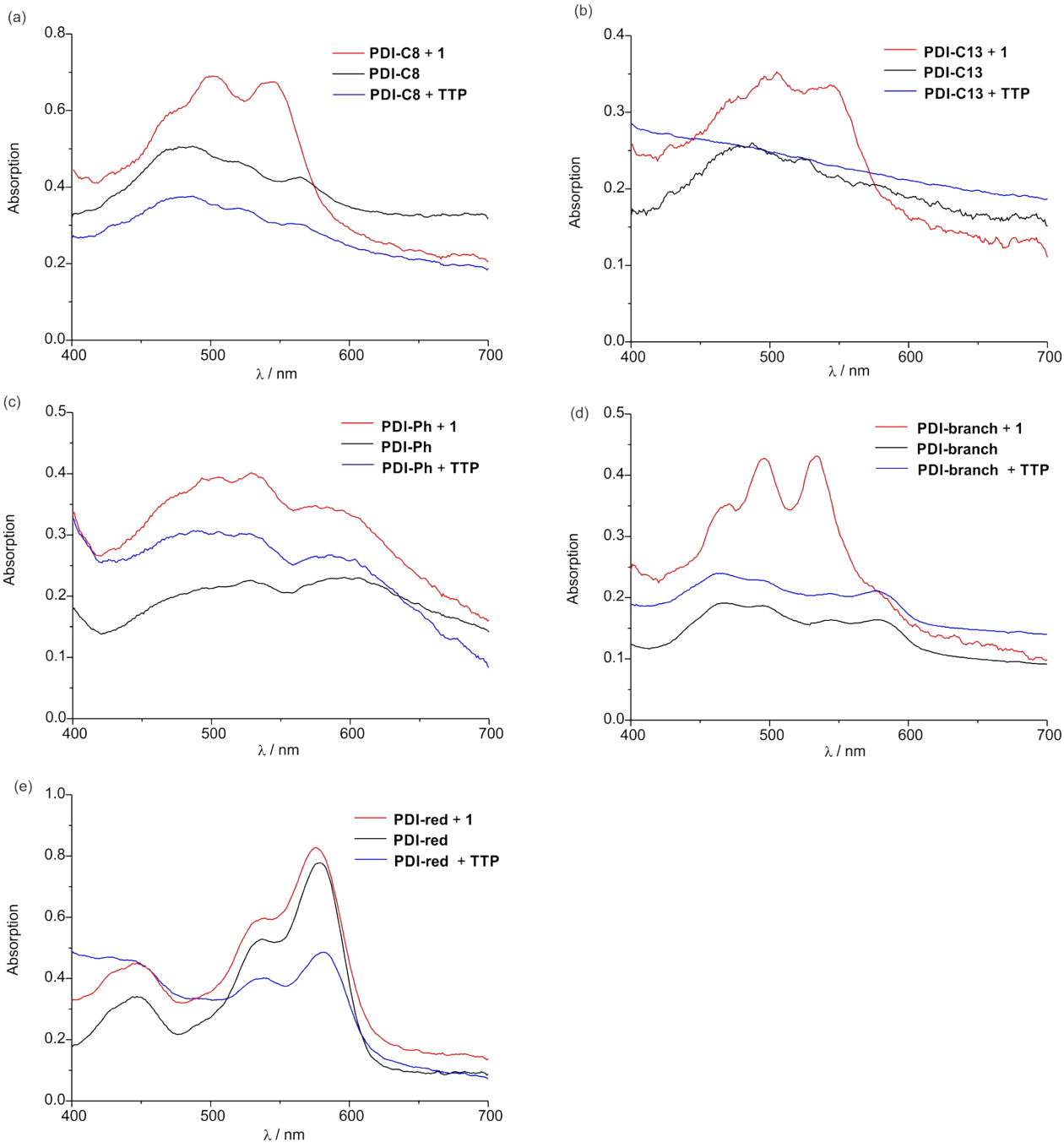

Figure S25. UV-vis spectra of film samples. (a) **PDI-C8**+**1** (black line), **PDI-C8** (black dotted line), **PDI-C8**+**TTP** (red dotted line). (b) **PDI-C13**+**1** (black line), **PDI-C13** (black dotted line), **PDI-C13**+**TTP** (red dotted line). (c) **PDI-Ph**+**1** (black line), **PDI-Ph** (black dotted line), **PDI-Ph** +**TTP** (red dotted line). (d) **PDI-branch**+**1** (black line), **PDI-branch** (black dotted line), **PDI-branch**+**TTP** (red dotted line). (e) **PDI-red**+**1** (black line), **PDI-red** (black dotted line), **PDI-red**+**TTP** (red dotted line). The molar ratio of PDI to **1** is 1 : 1 while PDI to **TTP** is 1 : 5.5 (equivalent to the weight ratio of PDI to **1**).

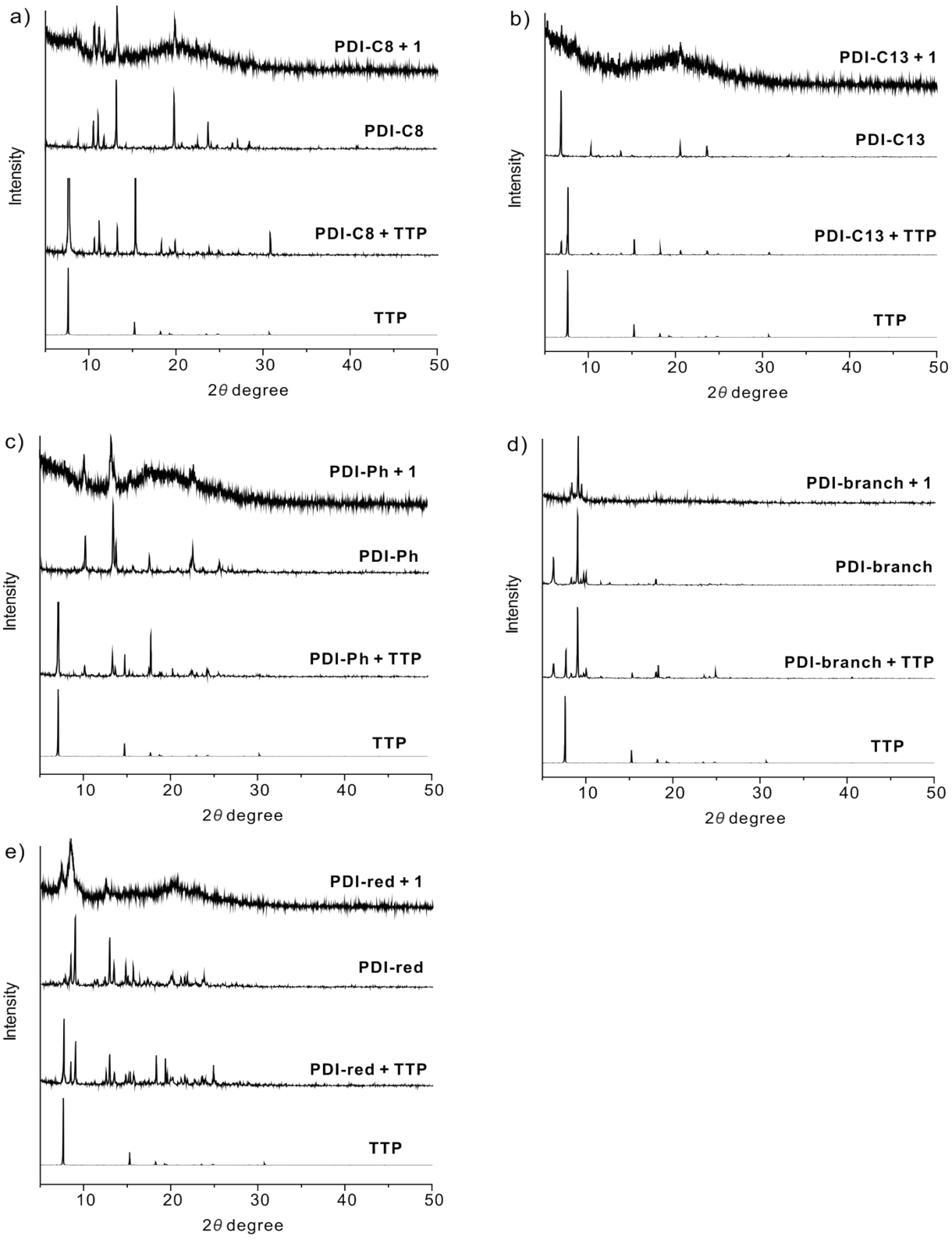

Figure S26. Powder X-ray diffraction spectra of PDI + **1**, PDI alone, PDI + **TTP** and **TTP** alone. The molar ratio of PDI to **1** is 1 : 1 while PDI to **TTP** is 1 : 5.5 (equivalent to the weight ratio of PDI to **1**).

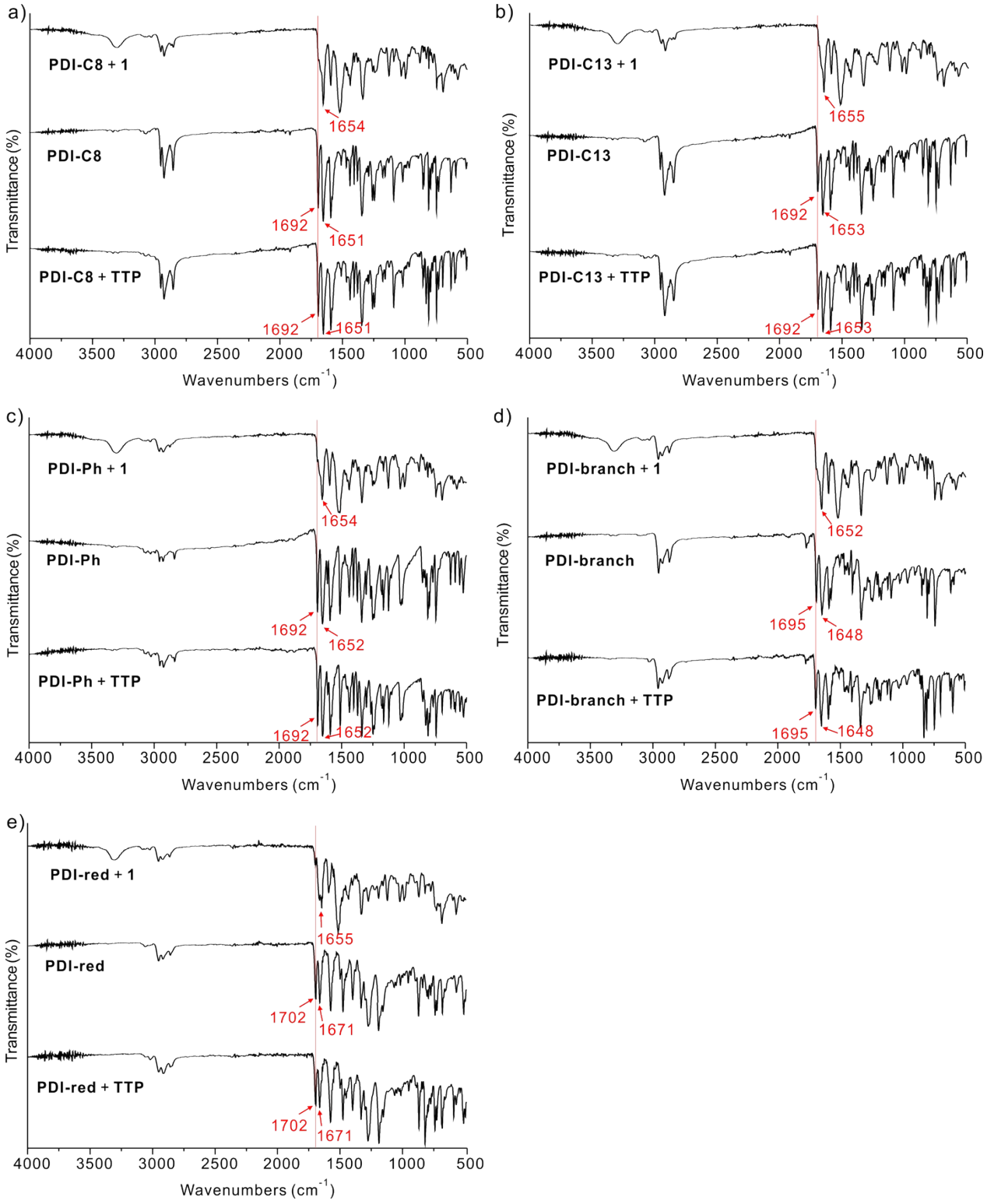

Figure S27. FT-IR spectra of the powder samples of PDI + **1**, PDI alone and PDI + **TTP**. The molar ratio of PDI to **1** is 1 : 1 while PDI to **TTP** is 1 : 5.5 (equivalent to the weight ratio of PDI to **1**).

1D NMR spectra

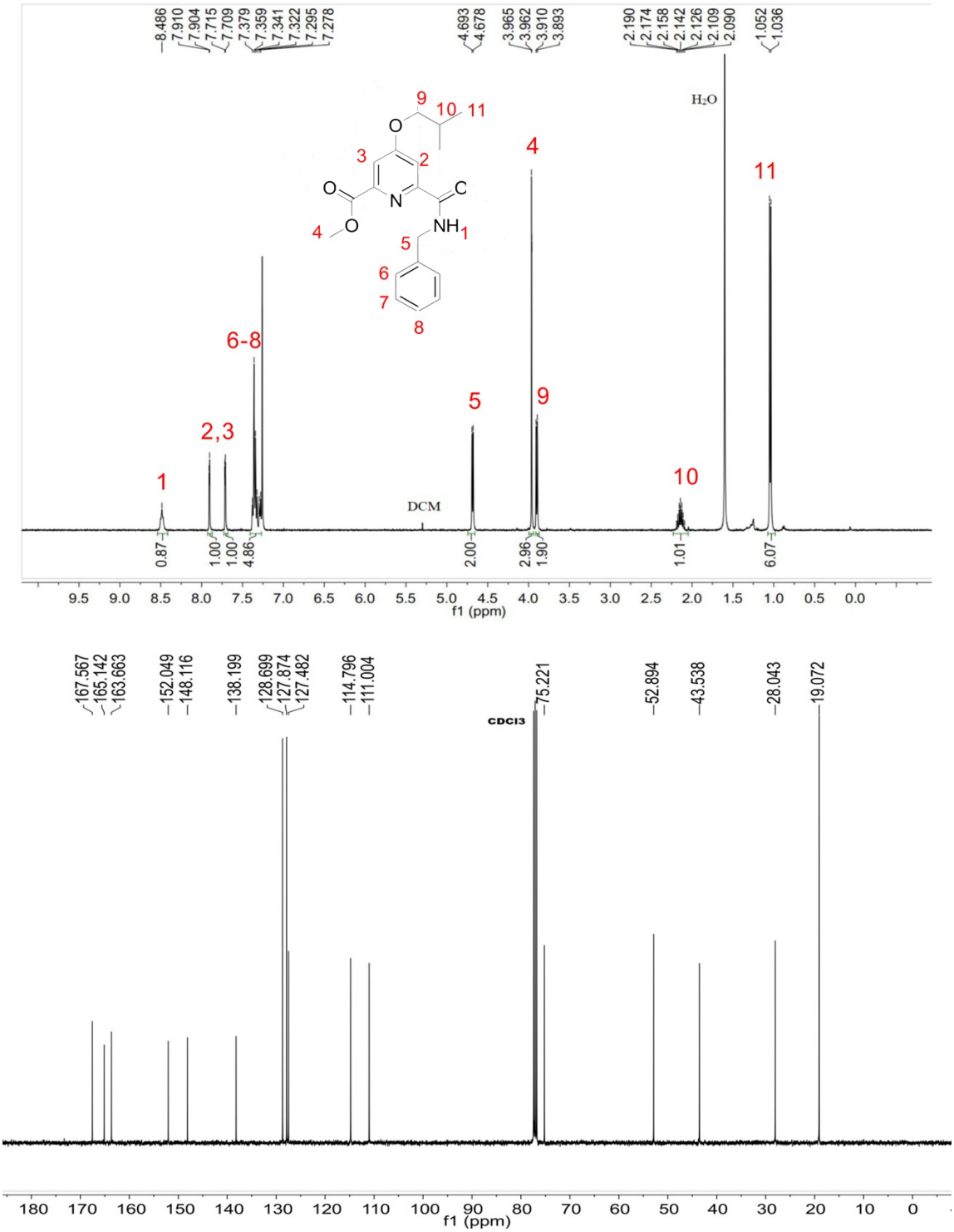

^{1}H NMR (400 MHz, $CDCl_3$) and $^{13}C\{^{1}H\}$ NMR (400 MHz, $CDCl_3$) spectra of methyl 6-(benzylcarbamoyl)-4-isobutoxypicolinate (**3**).

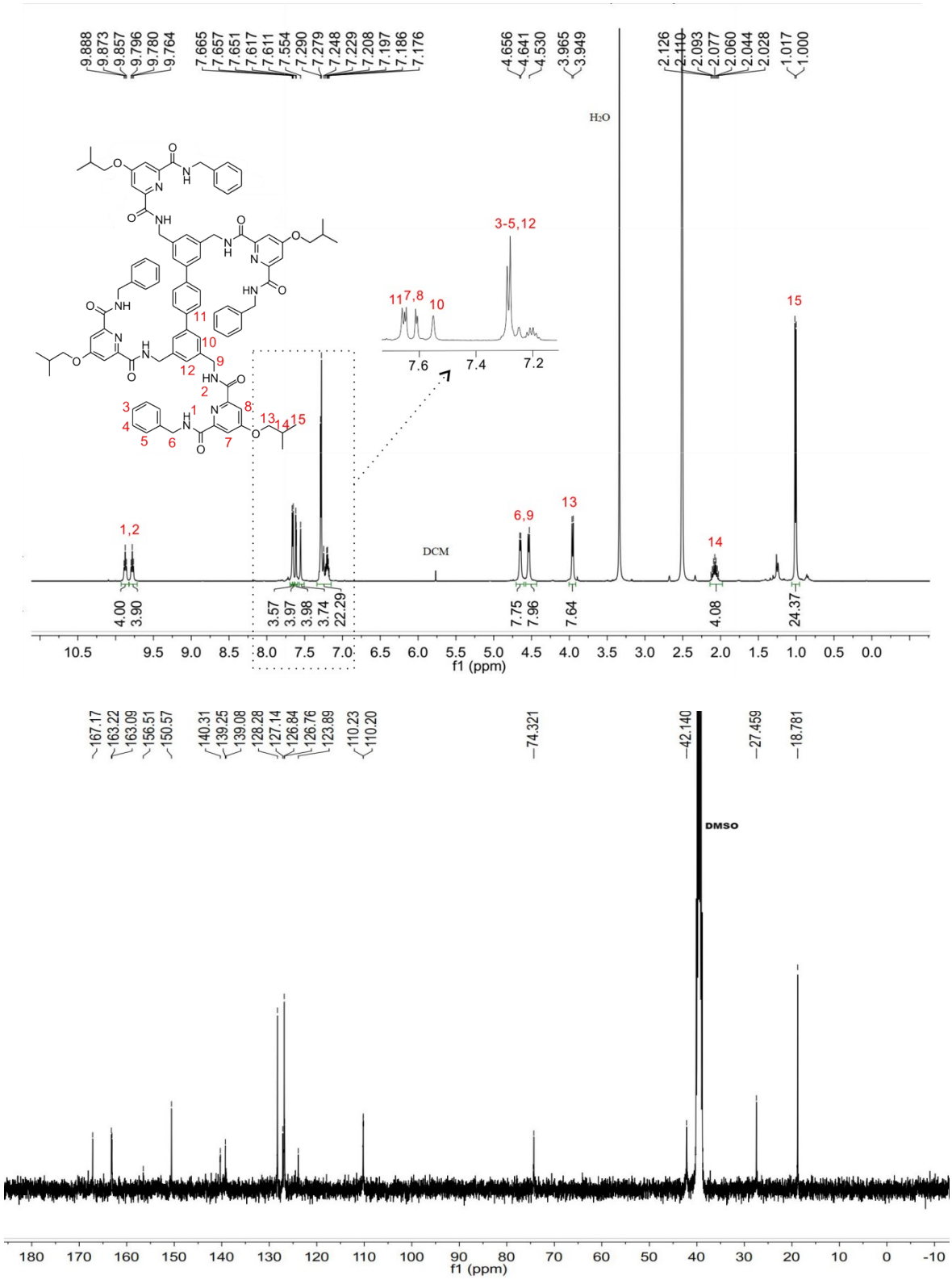

^{1}H NMR (400 MHz, DMSO-d_6) and ^{13}C{^{1}H} NMR (400 MHz, DMSO-d_6) spectra of the host (**1**).

Mass spectra

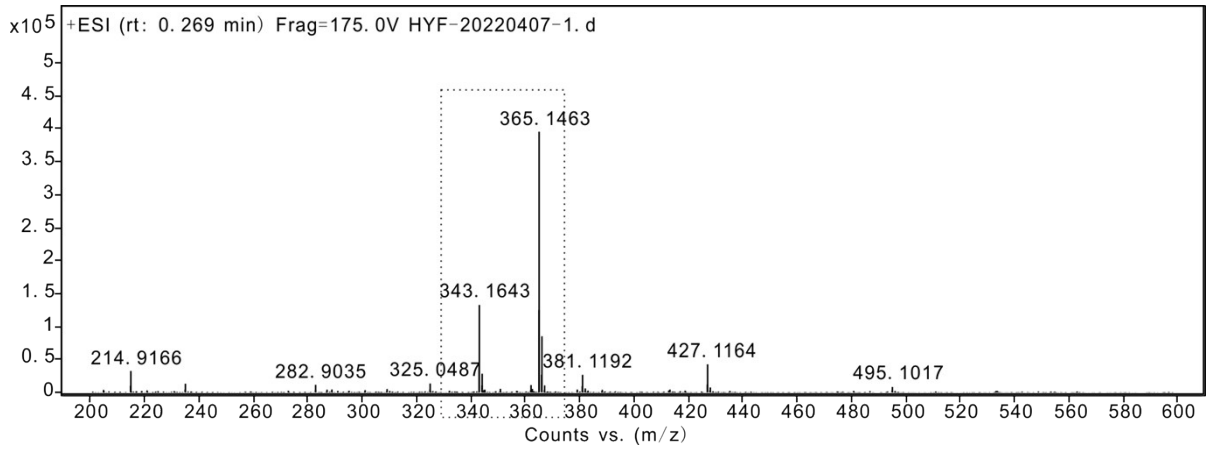

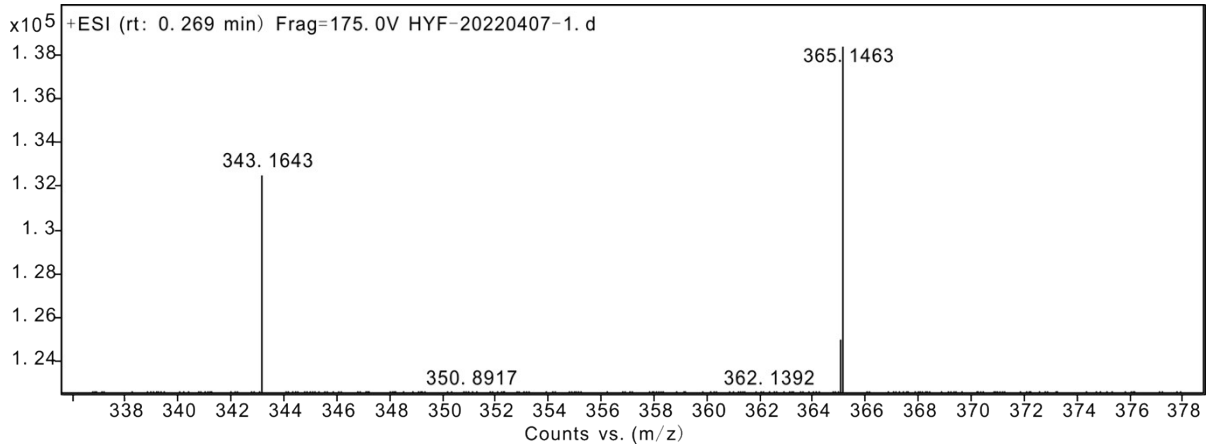

HRMS (ESI-TOF) of methyl 6-(benzylcarbamoyl)-4-isobutoxypicolinate (**3**), $[M + H]^+$: 343.1643 and $[M + Na]^+$: 365.1463.

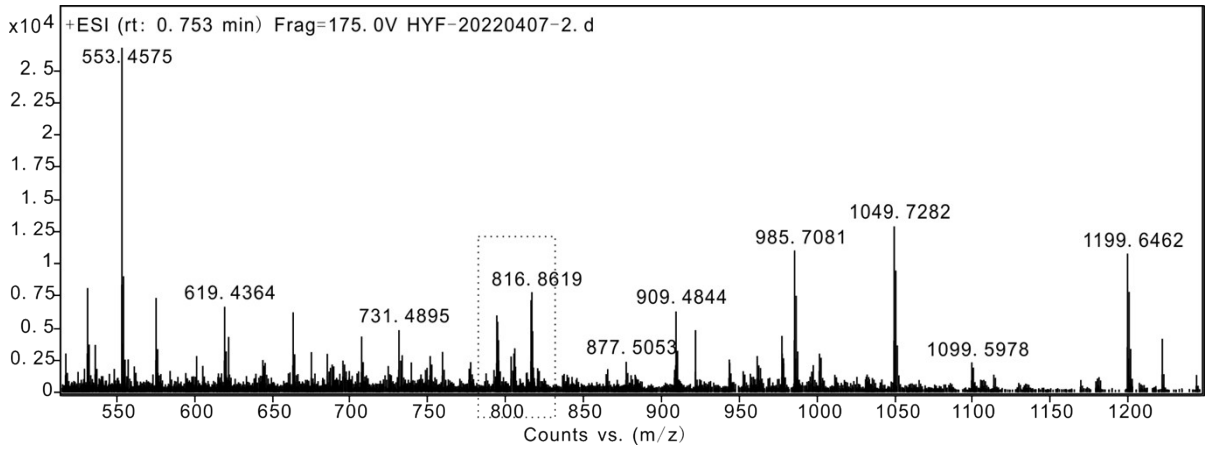

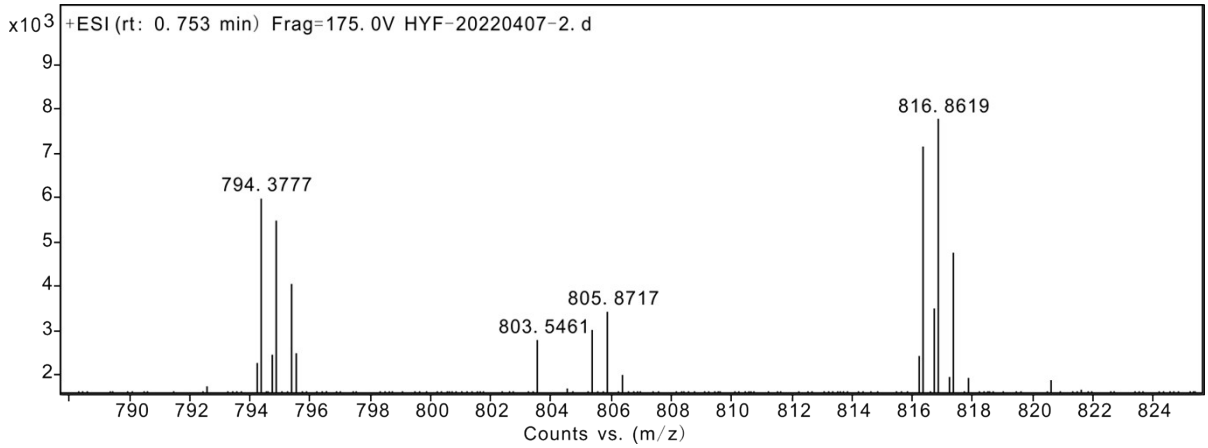

HRMS (ESI-TOF) of the host **1**, $[M + 2H]^{2+}$ (794.3777), $[M + H + Na]^{2+}$ (805.8717) and $[M + 2Na]^{2+}$ (816.8619).

References

( ) B. Baptiste, J. Zhu, D. Haldar, B. Kauffmann, J.-M. Léger and I. Huc, Hybridization of Long Pyridine-Dicarboxamide Oligomers into Multi-Turn Double Helices: Slow Strand Association and Dissociation, Solvent Dependence, and Solid State Structures, *Chem. Asian J.,* 2010, **5**, 1364-1375.

(2) G. Lecollinet, A. P. Dominey, T. Velasco and A. P. Davis, Highly Selective Disaccharide Recognition by a Tricyclic Octaamide Cage, *Angew. Chem. Int. Ed.,* 2002, **41**, 4093 - 4096.

(3) S. Alibert-Fouet, I. Seguy, J. F. Bobo, P. Destruel and H. Bock, Liquid-Crystalline and Electron-Deficient Coronene Oligocarboxylic Esters and Imides By Twofold Benzogenic Diels–Alder Reactions on Perylenes, *Chem. Eur. J.,* 2007, **13**, 1746 - 1753.

(4) E. Ämmälahti, M. Bardet, D. Molko and J. Cadet, Evaluation of distances from ROESY experiments with the intensity-ratio method, *J. Magn. Reson. Series A,* 1996, **122**, 230 - 232.

(5) a) P. Thordarson, Determining association constants from titration experiments in supramolecular chemistry, *Chem. Soc. Rev.,* 2011, **40**, 1305 - 1323; b) D. B. Hibbert and P. Thordarson, The death of the Job plot, transparency, open science and online tools, uncertainty estimation methods and other developments in supramolecular chemistry data analysis, *Chem. Commun.,* 2016, **52**, 12792 - 12805.